Intra-Logistics with Integrated Automatic Deployment:
Safe and Scalable Fleets in Shared Spaces

H2020-ICT-2016-2017
Grant agreement no: 732737

DELIVERABLE 4.4

Report on human injury data for autonomous mobile systems

Due date: month 54 (June 2021)
Deliverable type: R
Lead beneficiary: TUM

Dissemination Level: PUBLIC

Main authors: Mazin Hamad (TUM), Saeed Abdolshah (TUM)

Contents

Executive Summary

Prior to the autonomous operation of mobile robotic systems in the vicinity of human coworkers in shared workspaces, their safety aspects must be adequately investigated both qualitatively and quantitatively. More specifically, it must be well understood under which scenarios a collision between human and robot may be inevitable, and through which impact configurations the human gets injured. Also, the resulting trauma that may occur has to be identified, and its severity must be assessed. To address these issues, it is essential to make use of every available experimental information regarding injury biomechanics and (safe) tolerance levels for potential human-robot collision incidents. Moreover, enormous injury/safety data-sets covering various contact scenarios and impact arrangements are needed. However, even though standardized, uniform impact tests were earlier described to generate enough experimental knowledge regarding human injury biomechanics for safety in robotics (see e. g. [1]), the progress in this direction is unfortunately rather slow due to many obvious reasons. Consequently, in the context of ILIAD, we decided to compile an extensive literature review process regarding the human injury biomechanics. The goal is to collect, classify and digitize experimental impact testing findings from all publicly available sources of more than 75 years of research in forensics, automotive crashes, aviation, sports, military activities, falls, etc.

As a result, the gathered theoretical knowledge and practical experimental procedures from all reviewed studies and guidelines on injury evaluation through various testing setups and scenarios are introduced to robotics. This includes relevant data-sets encoding test characterizations, impact parameters, injury severity indices and classifications, together with their synopsis overviews. Based on the gathered data, a useful survey on the human injury biomechanics is made available to the robotics community, where a unified view on the experimental impact testing from a robotics perspective is provided. The proposed abstractions and developed procedures covering all human body parts, such that a complete human biomechanical injury model can be obtained. Useful insights and standardized protocols for carrying out crash-testing in robotics are provided and findings are continuously being communicated to the relevant standardization communities and their working teams on robot safety. A key finding of our exhaustive research review is the need for conducting more robot-to-human surrogate crash tests to generate more representative data-sets for safety in robotics.

1 Introduction

In recent years, physical human-robot interaction (pHRI) has become increasingly popular in both research and industrial applications. The close interaction between human and robot enhances the flexibility and productivity of processes. However, as contact is part of the process, undesired and potentially dangerous collisions may occur. Ensuring human safety is therefore a primary concern in pHRI. In robotics, the investigation of injury mechanisms and the development of safe mechanical designs and control strategies are ongoing topics and many efforts have been taken until now.

To enable active physical cooperation, operation regulations are imposed for all parties in Human-Robot Collaboration (HRC) systems [2], including machinery directives such as e. g. Directive 2006/42/EC for Europe [3]. In addition, safety standards that steer the mechanical design, task/motion planning and control of industrial and service robots are decisive to prevent any human injury. Some examples of these are e. g. the ISO10218/TS15066 for industrial robots [4, 5, 6], the ISO13482 [7] for personal care robots and ISO/TR 23482-1 [8, 9], in which safety-related testing methods and application guidelines are further detailed. In order to ensure respecting the relevant limiting thresholds, originating from extensive experimental impact studies as in e. g. [10, 11, 12, 13, 14, 15], novel algorithms and concepts for relating robot design and inertial properties to human injury and then human-safe control have been the basis for current safety standards of collaborative robotic systems [16].

A well-established biomechanics based safety approach was proposed in [12], where the authors suggested to relate the input parameters including reflected robot mass, velocity, and curvature with injury. This resulted in a well-established, unified framework, termed as Safe Motion Unit (SMU), for safe pHRI. For this injury analysis based approach, an energy shaping planner/controller guarantees that the resulting robot collision parameters are always human-safe. The systematic SMU scheme has been proven to be an effective solution for ensuring safety of robots with stationary bases, which was further strengthened through practical implementations into many stiff, heavy-weight industrial robot arms as well as light-weight torque controlled robot arms [17, 18]. Additionally, within ILIAD, SMU was extended to ensure human-safe operation of mobile autonomous systems in dynamic environments [19, 20].

In this deliverable, we focus on summarizing our long-running efforts to capture all relevant experimental information to human injury biomechanics and impact testing of more than 75 years of scientific research and experimentation. The findings of our extensive literature reviews focusing on identifying impact characterization, selection of subjects or test specimens, key collision scenarios, impact mechanisms and testing setups from relevant sources (automotive accidents, forensics, experimental crash tests, robotics, etc.) are summarized. As a result, a robotic perspective on experimental human injury biomechanics with detailed investigations, comprehensive data-sets and testing guidelines for different human body parts is provided. Based on this, we present the developed injury safety database with noteworthy insights into human injury related to autonomous mobile systems. Finally, we reflect our efforts to feed these valuable injury/safety data-sets into the according ISO committees, while representing an exhaustive extension of the existing "Handbook of Injury in Robotics".

2 Abstraction approach for experimental injury biomechanics and impact testing information and our unified robotics perspective

To generate ground-truth injury/safety data-sets needed for the data-driven robot safety frameworks such as the SMU, drop-test experiments with in-vitro pig specimens were previously suggested. Designing and executing these experiments was done in a systematic fashion to enable analyzing the effect of each robot-dependent parameter on the resulting injury and allow formulating appropriate safety criteria [12]. Consequently, a substantial amount of data was generated. However, in robotics and also in biomechanics, a lot of experiments have been conducted and reported. Those impact experiments and simulations usually differ in

- test setup, subjects, and measurements,
- analyzed injury (fracture, soft-tissue injury, pain etc.), and
- interpretation of results by means of the formulation of safety criteria.

Since collision experiments involve significant efforts, require ethical approval, and have a limited number of subjects, every experimental series and in fact every impact, provides valuable information on the human injury mechanisms with various body parts and their according tolerances. For the comparison of results and the development of future experiments, it is desirable to collect as much data and information from previous experiments as possible. We strive to represent collision data in a unified way and develop a database that comprises this data. This approach has following advantages:

- Results originating from different types of experiments and disciplines (robotics, forensics, biomechanics, simulations, etc.) can be compared easily.
- Different types of injury and injury quantification can be displayed, e. g. pain thresholds, medically observed skin injury, or biomechanical severity indices.
- The experimental conditions of the experiments as well as the resulting injury severity may be compared. Gaps can be identified to show where experimental data is still missing. In contrast, overlappings can be used to compare and verify results from different experiments. Contradictory outcomes may then be taken as an impulse to perform additional analyses.
- The collected data may be used to verify collision models and simulations.

Before delving into the body-part specifics regarding impact testing and injury biomechanics data summaries, we first introduce our proposed abstractions for unifying experimental information. The goal is to have a unified view on all collision mechanisms and impact scenarios involved in different experimental setups, for example free-fall, gravity-based drop tests, pneumatic testing machines, pendulum impacts, deceleration sled experiments, etc.

Depending on the type of restraining of the subject under test, one can distinguish between three different collision or impact scenarios: Unconstrained (U), constrained (C), or partially-constrained (PC) [21]. Note that this abstract set of standard collision scenarios is consistent with our previous work in the DLR's crash test series as visually depicted in Fig. 1.

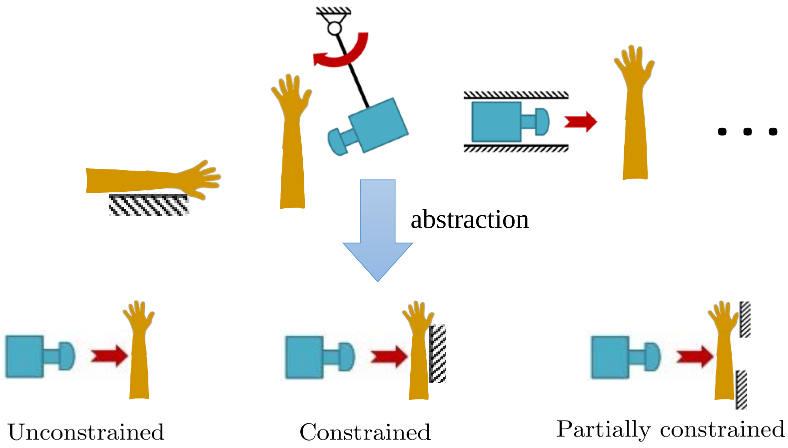

Figure 1: Standard collision scenarios. Collisions with a human arm is taken as examples for demonstration [22].

Moreover, the latter case, i. e. PC, is characterized only by a part of the subject being clamped which is not directly in contact with the impactor. Generalizing this categorization by considering also secondary impacts complete the abstraction of all collision scenarios that were considered in biomechanics experiments as depicted in Fig. 2.

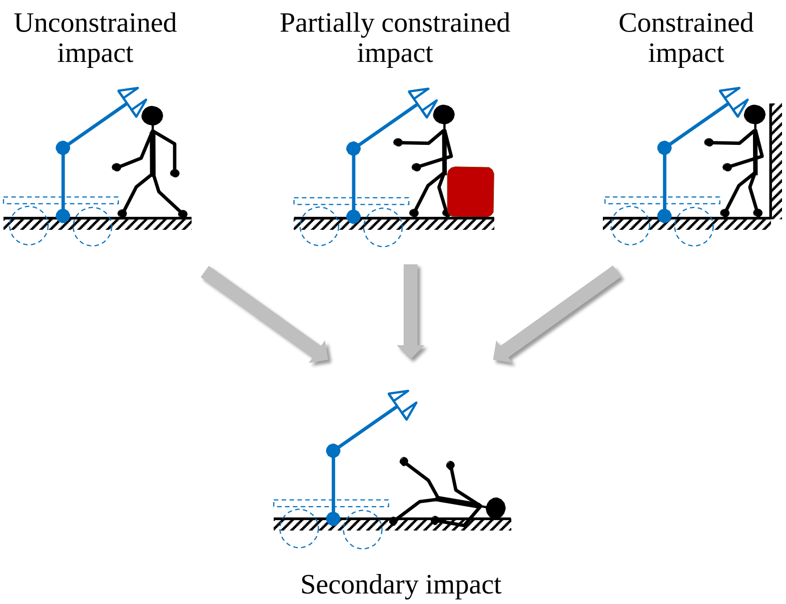

Figure 2: Classification of undesired/unintended contact scenarios between human and (mobile) robot.

By impact mechanism we mean the physical arrangement in which the collision is actually delivered to the test subject. In terms of test type, one can generally distinguish between three different categories of automotive crash tests (which also apply to non-automotive testing and certification procedures): Full scale tests, component tests, and single part tests [23].

In terms of loading type or impact velocity, one can distinguish between static, quasi-static and dynamic impacts. In an attempt to distinguish between these categories, Melvin et al. [24] classified 0.05 – 0.5 cm/s as quasi-static velocities and 3 – 5 m/s as dynamic impacts. Furthermore, Bilo et al. [25] defined static loading as a relatively slow impact of forces exerted over a protracted period (> 200 ms), which occurs when the skull is squeezed and compressed. Moreover, the authors attributed dynamic (or rapid) loading with the case when the impact of forces is exerted over a shorter period (<200 ms, often even less than 50 ms). However, to the best of our knowledge, there is no well-defined distinction between the three impact velocity ranges.

Regarding abstracting the curvature information at impact location, we adopt the set of basic impactor geometries developed by Haddadin et al. [12] for their early drop-tests with pig specimen at the DLR, see Fig. 3. Note that the z-axis of each of these impactors is aligned with the direction of impact during experiment, with the following surface curvature parameterization: Radius, edge radius, length/width/height, angle, and padding characteristics. Moreover, different sharp tools were used by the same team in another series for experiments involving soft-tissue injuries [26], see Fig. 4.

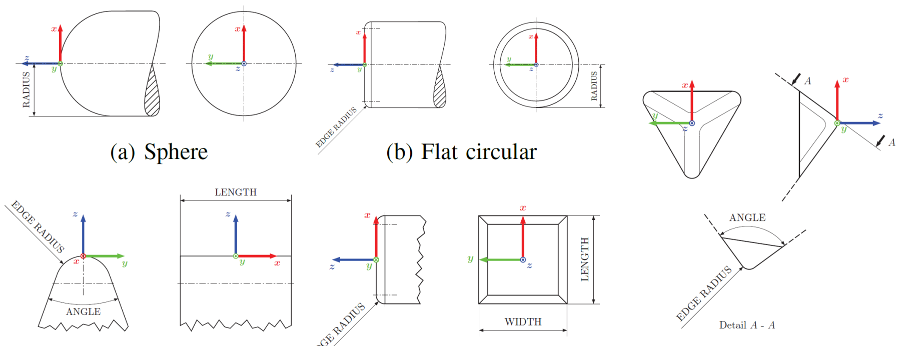

(a) Sphere (b) Flat circular (c) Edge (d) Cuboid (e) Pyramid

Figure 3: Impactor curvature and key surface primitives.

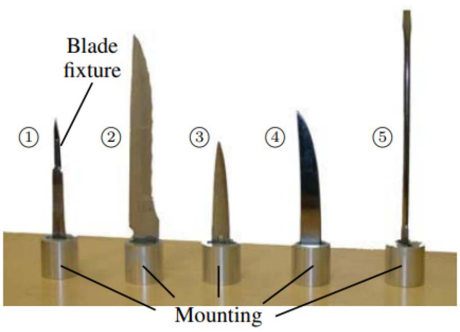

① Scalpel, ② kitchen knife, ③ scissors,
④ steak knife, ⑤ screwdriver.

Figure 4: Sharp impacting tools.

3 Experimental impact testing data

For further categorizing the experimental impact incidents/tests, we propose principal impact setups involved in generating the collision incident. An impact setup encodes the specific physical arrangement (e. g. horizontal or vertical) and mechanical acceleration machinery, i. e. accelerated impactor mass versus accelerated human (surrogate) body part, that is employed in order to generate the collision incident. As a result, basic principal setups were identified that cover all impact configurations. Figure 5 shows an example of such set of principal impact setups, with the difference between each pair is whether human body part or impactor apparatus was accelerating. Note that the shown arm is chosen just an example and this principal impact setups may also be valid for other body parts. Typically, this abstract set of principal impact setups, together with standard collision scenarios, loading type and impact curvature characteristics is suitable for describing contacts with the head, thorax and abdomen, as well as with upper extremities (i. e. arm and hand).

The injury tolerance level/criterion is understood to be an upper bound, limiting value that is derived from statistical analysis [27] or empirical data [28], which delimits dangerous collisions from safe contacts. In the following we provide synopsis plots summarizing the experimental findings in terms of measured physical impact quantities versus fracture/injury tolerances for various human body parts, whereas more elaborated abstractions are first introduced when necessary.

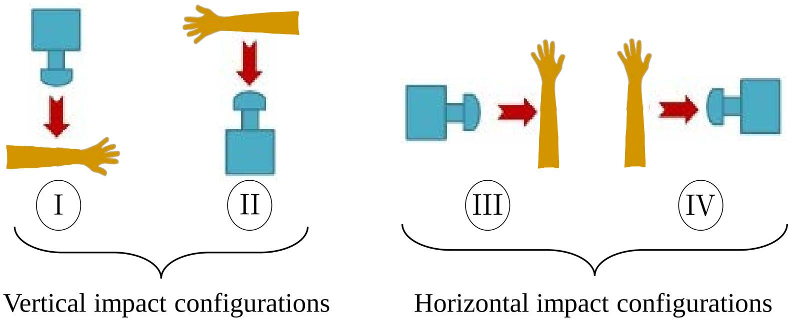

Figure 5: Principal testing setups for impacts with a human arm [22].

Injury tolerance level/criterion is understood to be an upper bound, limiting value that is derived from statistical analysis [20] or empirical data [128], which delimits dangerous collisions from safe collisions.

- Head, thorax and abdomen

  Figure 6 demonstrates a synopsis plot for the reported range of fracture forces, i. e. exceeding the bone tolerance levels, in biomechanics literature for different head regions.

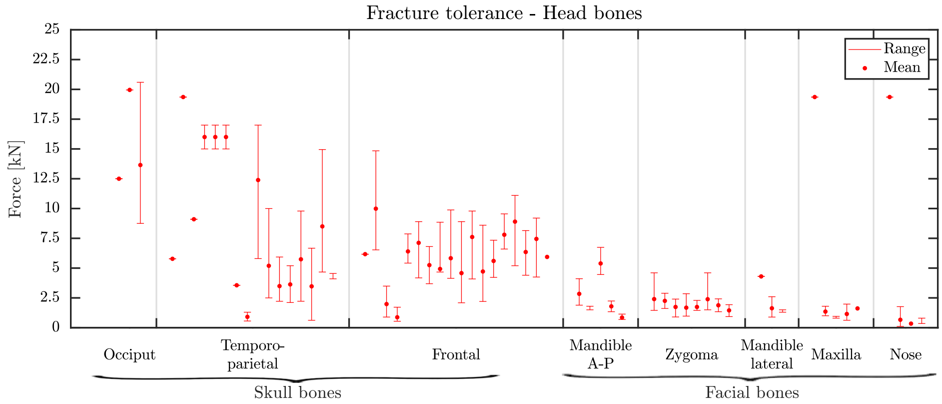

Figure 6: Synopsis plot for fracture forces of the head cranial and facial bones in the reviewed impact biomechanics studies. The dot indicates the average value of the reported force values.

The mass/velocity representations for head impact experimental findings from biomechanics literature with usable data-sets for safety in robotics are provided in Figs. 7, 8, 9 and 10 for various impactor curvatures.

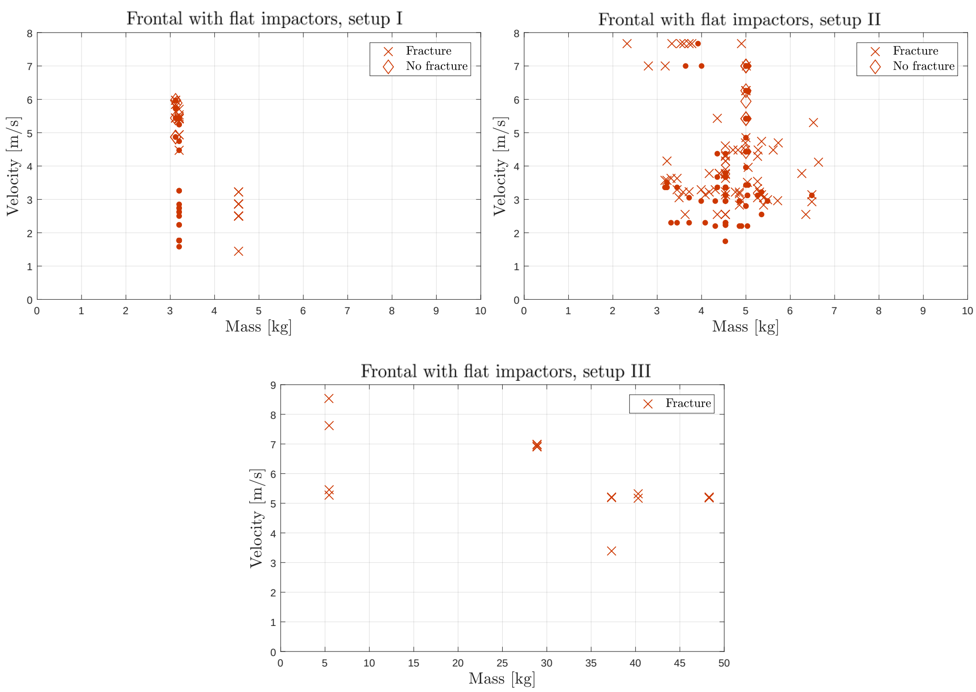

Figure 7: Summary of relationship between mass, velocity, and injury for experiments in the literature on the frontal bone with setup I (upper left), II (upper right), III (lower left) and with all setups combined (lower right).

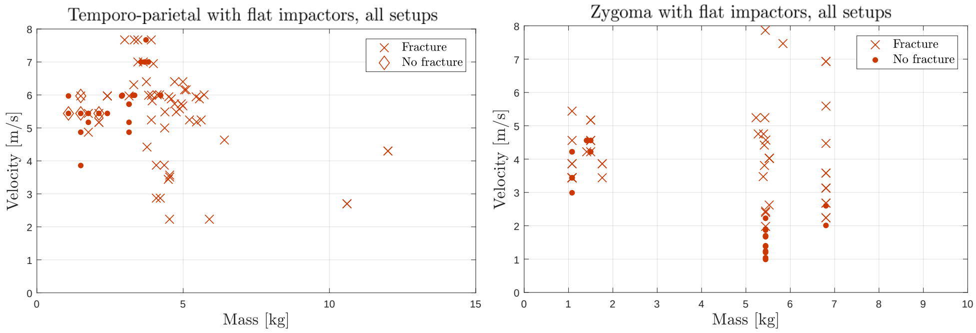

Figure 8: Summary of relationship between mass, velocity, and injury for experiments in the literature on the temporo-parietal bone (left) and the zygoma (right).

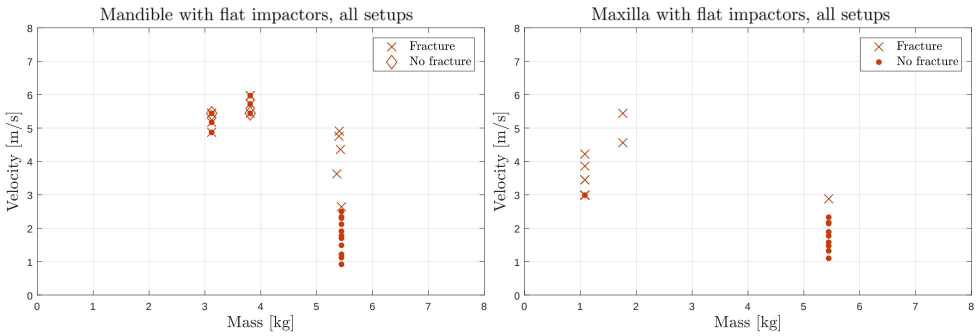

Figure 9: Summary of relationship between mass, velocity, and injury for experiments in the literature on the mandible (left) and the maxilla (right).

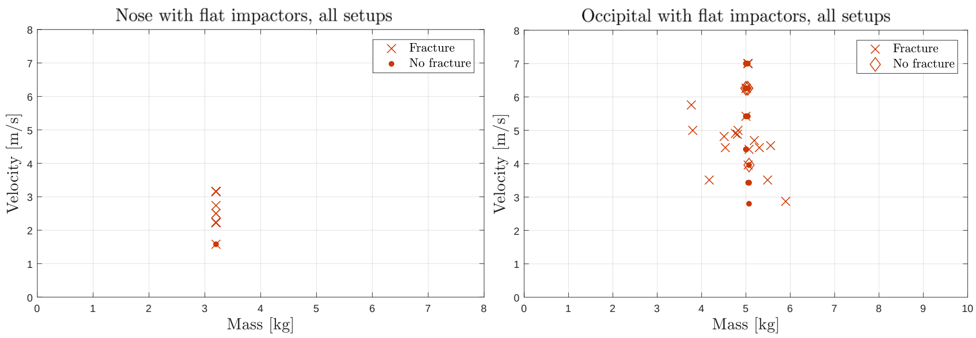

Figure 10: Summary of relationship between mass, velocity, and injury for experiments in the literature on the nose (left) and the occipital bone (right).

Figure 11 demonstrates a synopsis plot for the chest injury tolerances estimated based on the deflection (i.e., compression) and viscous criterion reported in the reviewed biomechanics literature.

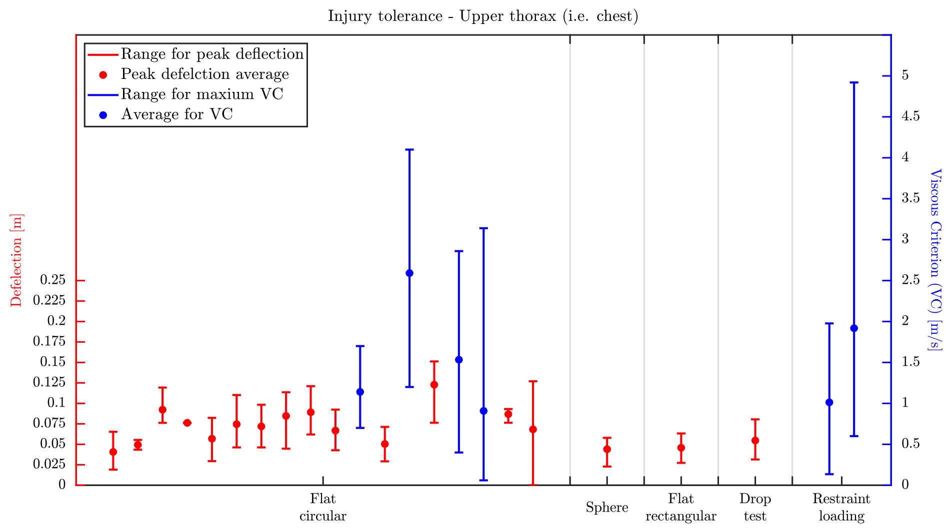

Figure 11: Synopsis plot for chest injury tolerances in the reviewed impact biomechanics studies. The dot indicates the average value of the reported values.

The mass/velocity representations for head impact experimental findings from biomechanics literature with usable data-sets for safety in robotics are provided in Fig. 12 for various impact setups.

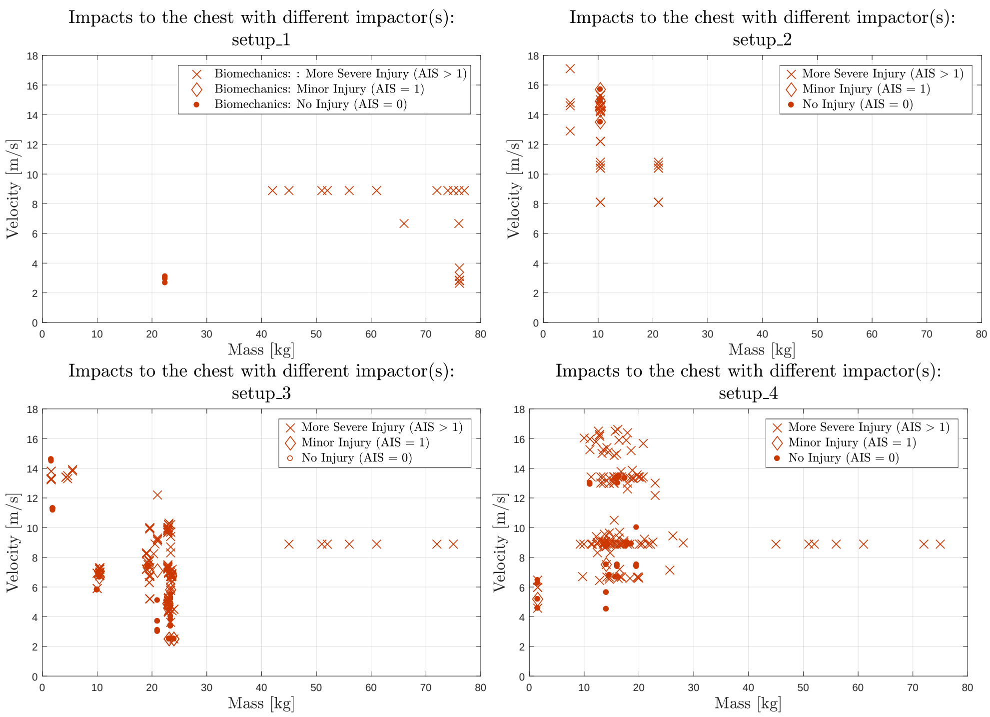

Figure 12: Summary of relationship between mass, velocity, and injury in biomechanics literature for different impact setups of experiments on the chest with: setup I (upper left), II (upper right), III (lower left) and setup IV (lower right).

Only a few studies have been carried out to determine the injury tolerance of abdomen [29, 30, 31, 32, 33, 34]. These studies do not come to a common consensus on a tolerance limit for the abdomen in general. This is due to the complex structure of the abdomen. Studies have covered different regions and/or quadrants making it difficult to compare results. As a result, of the extensive literature review, various tolerance limit values were found inconsistent with each other to a great extent. Nevertheless, our chosen injury criteria and their tolerance values of the abdomen region from the reviewed studies are presented in Tab. 1 together with those for the thorax.

Region	Criterion	Tolerance value	Reference
Thorax	acceleration	60 g	[35]
	force	3.3 kN	[36]
	force (pain)	1.7 kN	[37]
	compression	22 mm	[37]
	viscous	0.5 m/s	[28]
Abdomen	acceleration	75 g	[38]
	force	4.4 kN	[33]
	compression	60 mm	[33]

Table 1: Injury tolerance limits for thorax and abdomen.

- Neck

  Concerning the neck, a classification of experimental setups used in the literature is proposed taking into account the different loading directions. An overview can be seen in Fig. 13, where the majority of collision scenarios are partially constrained impacts, since the torso is normally fixed to the test frame but the head and neck structure can move freely.

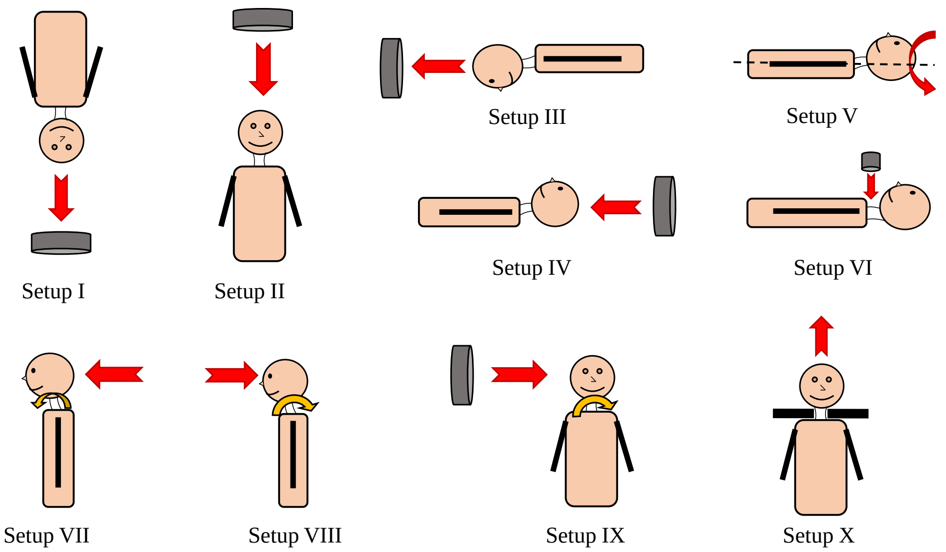

Figure 13: Abstraction of the experimental setups used in the literature to study the neck injury biomechanics.

Constrained scenarios are usually produced when isolated cervical spines are tested or when quasi-static tension loads are applied. Unconstrained scenarios are common in Setup I when postmortem human surrogates (PMHSs) are dropped to produce compression impacts, or in Setup IV when the subject is placed on an horizontal position and no constraint is fixed in the direction of the application of the loads. The latter case can be observed in Fig. 14a, while the same test setup in a partially constrained scenario is represented in Fig. 14b.

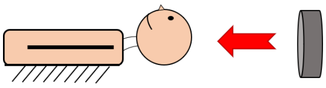

(a) Unconstrained

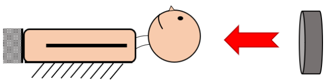

(b) Partially constrained

Figure 14: Different impact scenarios of Setup IV

In the case of the sled tests present in Setups VII and VIII, the torso of the subject is usually constrained using a three-point seat belt, as the intention is usually to simulate loadings present in a car collision. In some tests, a head-rest is also used. This constrains the backward movement of the neck, but it still allows the head to move in the forward direction. The partially constrained scenarios using sled tests can be seen in Fig. 15a for Setup VII andFig. 15b for Setup VIII.

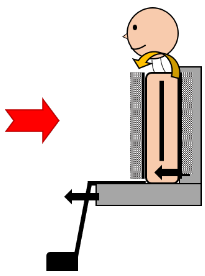

(a) Setup VII

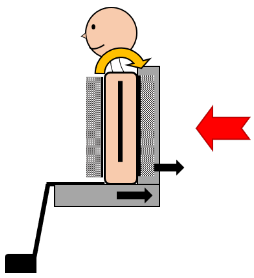

(b) Setup VIII

Figure 15: Different sled test scenarios with partially constrained subject

The synopsis plot for the forces directly applied to the head or neck of the specimens is shown in Fig. 16 where different loading types are presented together. For this synopsis plot and all the similar upcoming ones, the light-colored bars denote the lower and upper reported values, whereas the asterisk symbol marks the mean value and the darker bars encode the 3-σ (99.7%) standard deviation for the specific experimental series. In case experimental findings from crash test dummy studies are shown in the synopsis plot, they are denoted in the legend with ATD (which stands for "anthropomorphic test device").

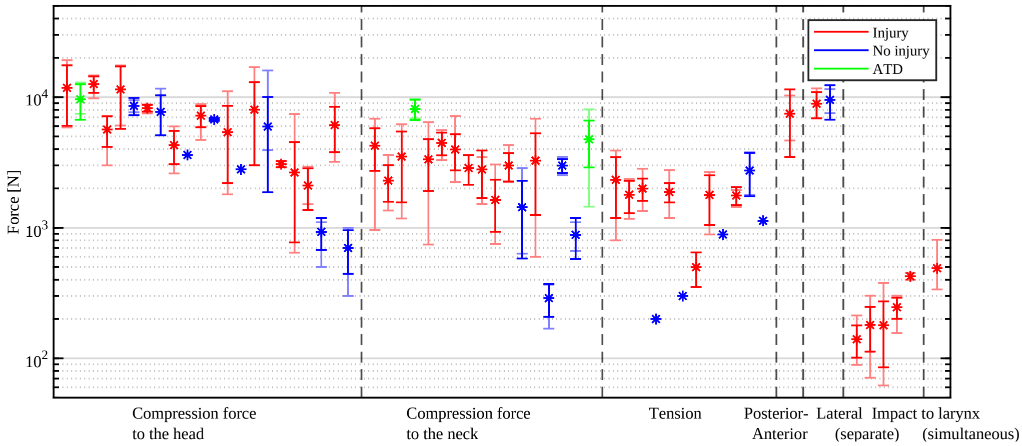

Figure 16: Synopsis plot of applied forces to the head and neck from the reviewed experimental neck impact studies.

The synopsis plot for the moments at the occipital condyles of the specimens for different bending types is shown in Fig. 17

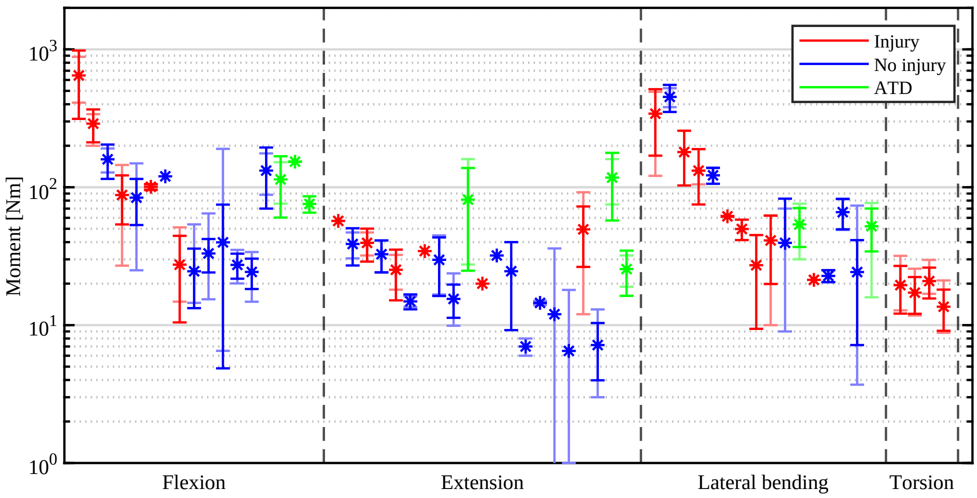

Figure 17: Synopsis plot of resulting moments at the occipital condyles from the reviewed experimental neck impact studies.

The synopsis plot for the shear forces at the occipital condyles of the specimens for different bending types is shown in Fig. 18

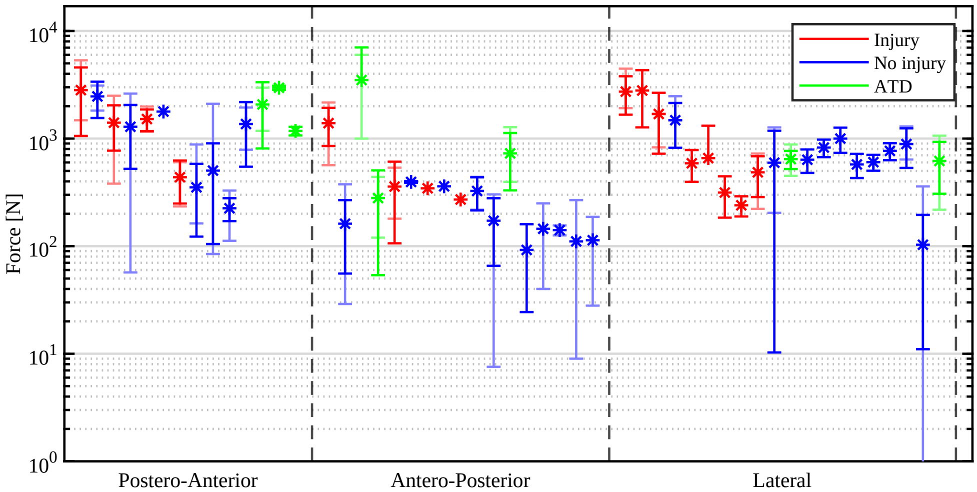

Figure 18: Synopsis plot of resulting shear forces at the occipital condyles from the reviewed experimental neck impact studies.

The synopsis plot for the Neck Injury Criteria (NIC) values of several impact experiments is shown in Fig. 19. Since each impact scenario (frontal, rear-end or lateral collision) requires a different criterion, different criteria are selected depending on the provided information (forces and moments at the occipital condyles or at the base of the neck). A value of 1.0 is set as the injury threshold for all the criteria except from the Lower Neck Injury Criterion (LNij), in which the threshold value is 1.1. This value is associated with the probability of 50% of having AIS1 injury [39]. For the Beam Criterion (BC), the value of 1.0 is also associated with a 50% of AIS1 injury risk [40]. For the normal Neck Injury Criterion (Nij), a value of 1.0 is assigned to a probability of 30% of AIS2 and 22% of AIS3. Since the injury criteria are probabilistic methods and do not define a determining threshold for predicting the level of injury, as can be derived from the synopsis plot. The criterion that seems to perform better according to the available results is the Neck Protection Criterion (Nkm) for rear-end collisions.

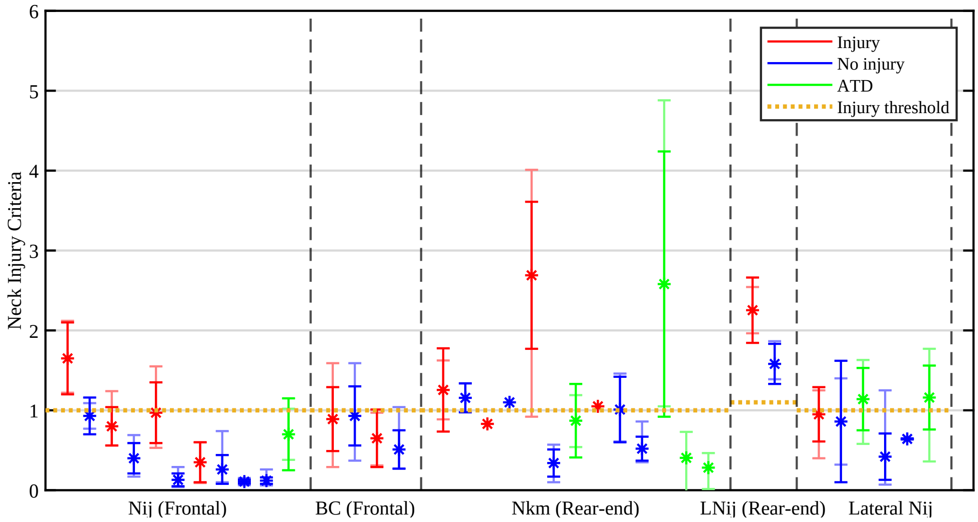

Figure 19: Synopsis plot summarizing the reported NIC values from the reviewed experimental neck impact studies.

In Fig. 20, the mass-velocity plot for the neck based on the literature review is shown. In it,value pairs resulting in injury are plotted together with pairs producing no injury for several experiments.

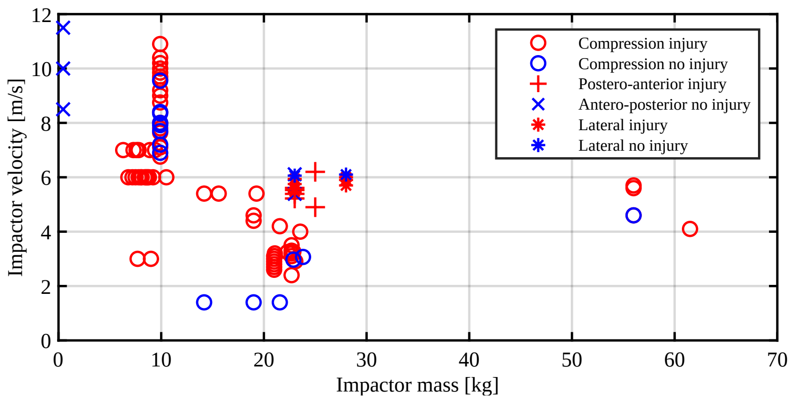

Figure 20: Mass-velocity versus injury for the neck from the reviewed experimental neck impact studies.

- Upper extremities

  An overview of the reported force values of various loading tests within our massive list of reviewed references for biomechanics impact data is given Fig. 21. We note here that the reported human arm/hand injuries are mostly fractures, which can results from collisions with bulk robots or near singular configurations, enduring a (quasi-)static loading on the human upper extremity or during a secondary following impact after the initial crash. Fewer fracture injury data-sets from dynamic impacts were encountered in the extensive literature we reviewed, see Fig. 22. However, injuries milder than bone fractures, which may provide criteria suitable to the more light-weight robots, requires more collective effort to carry out further specific experimental investigations. Regardless of the different experimental conditions, a trend for each body part is visible. The long bones' experiments show that the necessary fracture force for all of them is in the same region. In [41], it was also concluded that the force onset direction, Lateral-Medial (LM) or Anterior-Posterior (AP) direction, is not relevant for a single bone, e. g. the humerus in this case. Regarding the Colles fracture of the wrist, there is no clear threshold resulting from Fig. 21. There, a synopsis plot of the force values reported in the reviewed experimental data sources, that mostly investigate fracture injuries, is given. Red color means that fractures occurred and blue means no injuries, e. g. while tests with volunteers. The asterisks mark the mean values, the solid lines represent the standard deviation and the light colored lines depict the range between lowest and highest values. Humerus, forearm, ulna and radius are tested in three-point bending tests, wrist means the human falling on hands setup, and finger denotes the jamming in closing car window arrangement. At the bottom, the mass-velocity plot shows the results of drop tower experiments. Red colored marks mean that in all tests injuries occurred at this mass-velocity combination of the impactor. If both, fractures and no injuries, were resulting the mark is colored magenta. Humerus and forearm are results from three-points bending tests, wrist means the human falling on hands setup, and elbow is similar to three-point bending tests, but with overextending the elbow joint.

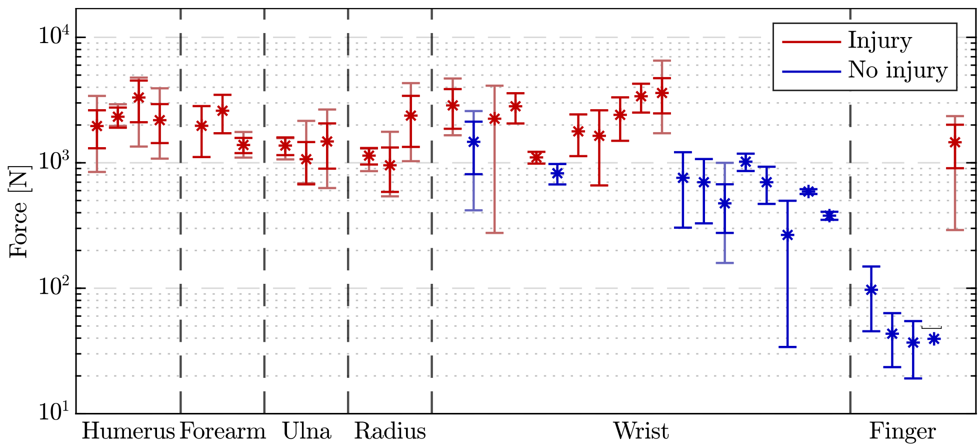

Figure 21: Synopsis plots of the reported force values versus injury in reviewed experimental impacts with the human upper extremities.

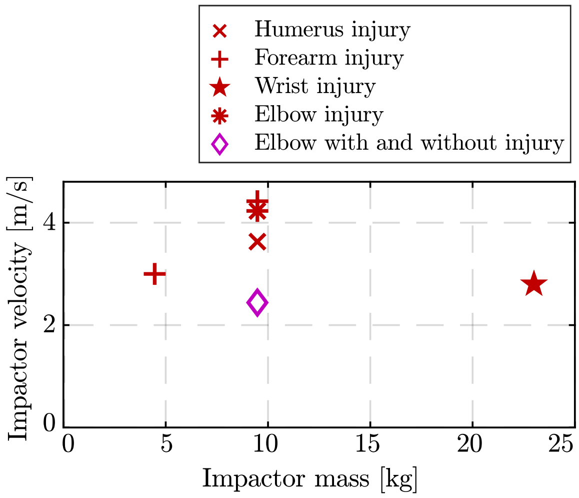

Figure 22: Mass-velocity versus injury in reviewed experimental impacts with the human upper extremities.

- Lower extremities

  To facilitate the application of injury data in robotics applications, the various setups and scenarios of impact tests discovered from the literature are summarized in Fig. 23. In the top row, different test setups are condensed to four main categories. The categorization of different impact tests for lower extremities are shown in Fig. 23 (middle and last rows). This variety of impact tests can cover different collision scenarios of human with a mobile robot. The proposed abstractions paves the way to apply the injury data in robotic scenarios and replicating the experiments for robotic applications.

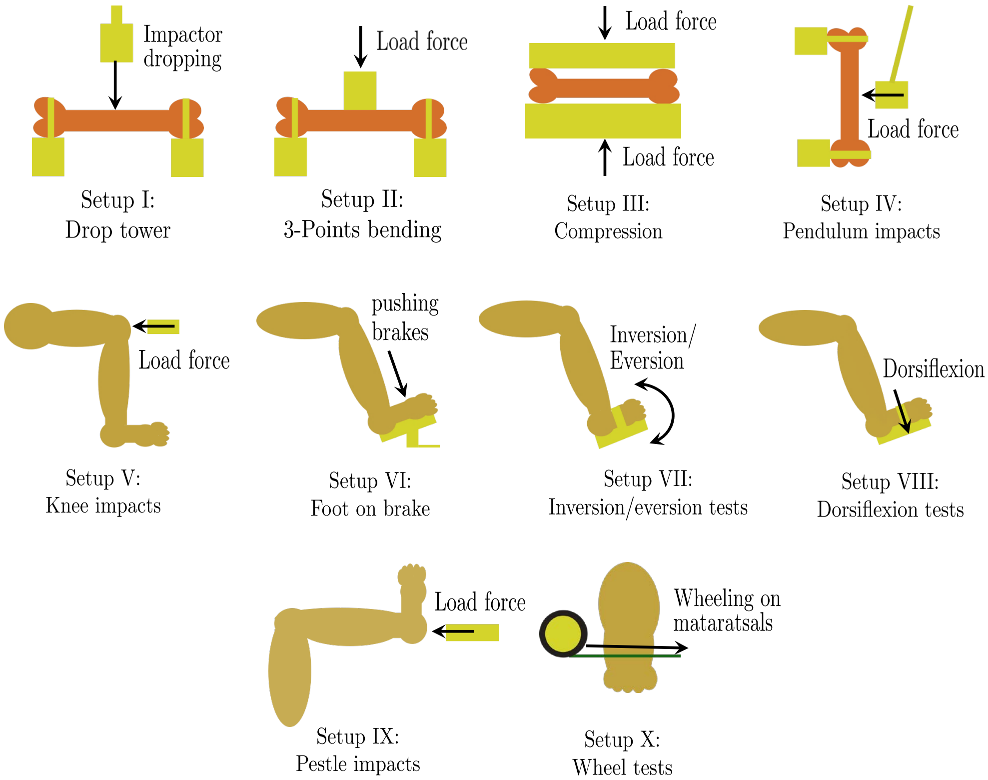

Figure 23: Abstractions of the various impact setups for the human leg and foot.

The synopsis plots shown in Fig. 24 present the reported impact force/torque in experimetnal impacts to human lower extremities (i. e. leg or foot) is expected to occur. Generally, the force level thresholds for the lower extremity bones are in a range between 1 kN and 10 kN. A particular exception is the fibula, whose threshold is around 300 N. Both force and torque plots confirm that fibula is the weakest part of lower limbs; however, knee is resistant against fairly large magnitude of force/torque. The presented data is specifically useful for design and control of mobile robots.

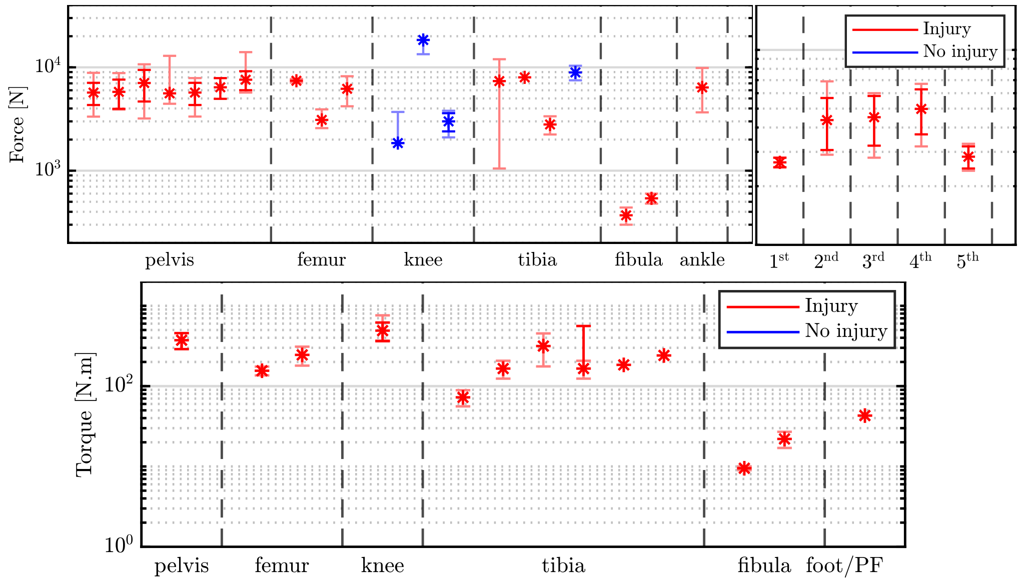

Figure 24: Synopsis plots for the observed force and torque limits of human lower extremities.

Figure 25 shows under which impactor mass and velocity the human leg injury may happen. In a robotic application this can be translated to under which robot reflected mass and velocity a collision causes injury.

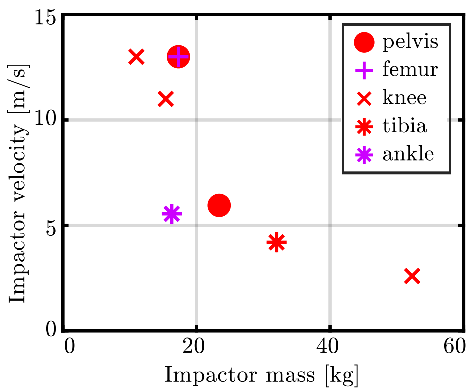

Figure 25: Mass-velocity versus injury/safety for the human leg based on previous studies.

4 Generating robotics relevant data experimentally

Blunt impact injury experiments and its characterizing relevant factors to robotic impacts can be drawn from the automobile industry crash-tests. Since car industry has been in the public market for more years than robotics, its results are robust and have been tested on real-life safety solutions, e.g. safety belts and airbags in a car. The issues of applicability to robotics and extrapolation of results arise with this approach, due to the differences in velocity and mass ranges of tested apparatus. Moreover, generating experimental data-sets for the impact curvatures encountered with various robot edges/end-effector tools (possibly sharp) is necessary.

4.1 Pendulum impact tests

The ISO/TS15066 standard on collaborative robots [6] proposes a simple model to calculate the effective mass of a robot contributing to the impact energy. In contrast to its proposed simplified model, there is an analytical model based on the robot dynamics. We evaluated whether the simplified model is appropriate and how the dynamics model compares to reality using a passive pendulum set up, see Fig. 26. This setup measures the pendulum speed after colliding with the robot using a light barrier and enables us to calculate the effective mass. As a result, the effective mass model from ISO/TS 15066 shows high variations from the real data; however, our the analytical model demonstrated promising results [42, 43].

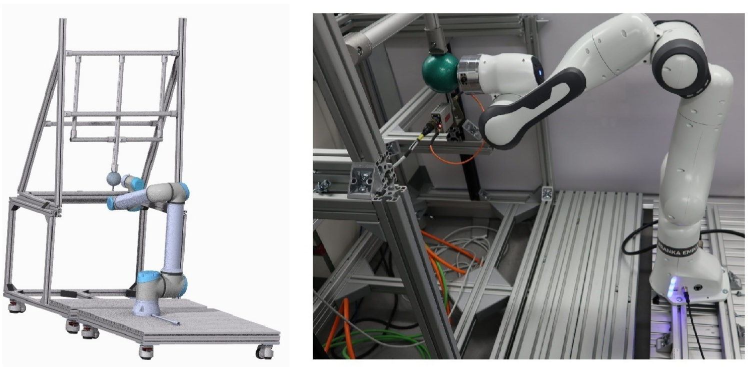

Figure 26: Pendulum setup to validate the robot effective mass during impacts [42, 43].

4.2 Drop-tests

To complement the crash-testing results usable for robot safety studies, drop-tests were performed in [12]. The drop-tests were performed with porcine specimens against different contact surfaces and penetration depth with sharp tools. Porcine subjects are widely used in impact studies [44, 23, 45, 46] due to the high resemblance of a pig skin to that of humans in most aspects relevant to the studies of impacts for some regions, e. g. the abdominal layers seen in Fig. 27, center. The developed testing approach was chosen in order to generalize the test results. The impact mechanism used in these experiments is shown in Fig. 29, left.

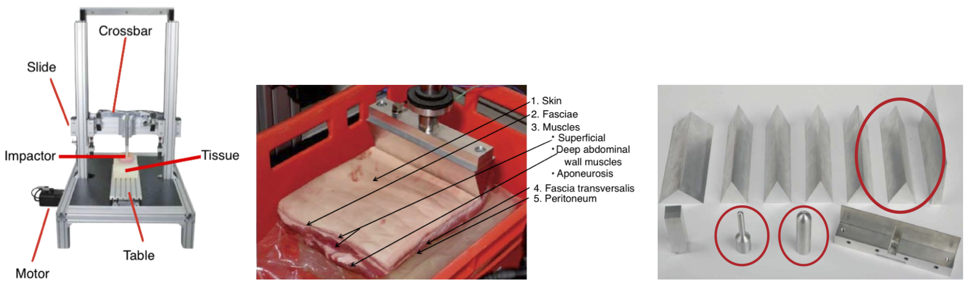

Figure 27: Pig skin layers (left) used with the drop-test setup for impact experiments (center) and their according primitives (right) [12].

In order to produce injury/safety data-sets that can are usable with a wider variety of end-effector tools, a set of primitives was used for the experiments, see Fig. 27, right. Then, these primitives and their results were combined to get the parametric results (factors that induce a type of injury) for more complex end-effector tools. Thus this is a more generic way of approaching the problem for getting more meaningful data that can be used for applications.

Each drop-test impact result was analyzed and categorized so as to determine the resulting skin, muscle and nerve and vessel injury. Quantification was done by means of medical assessment and use of a standardized metric for injury classification, namely the AO classification. Care needs to be taken when choosing the injury index to be used. Dealing with the injuries incurred by impacts with the end-effector tools. The most common injuries in robotics are closed skin injuries [47], which should serve as the limiting criterion for the injury classification. In Fig. 28 the assessment of closed injury (IC) according to AO-classification is depicted as a mass-velocity relation plot, so called *risk curve*.

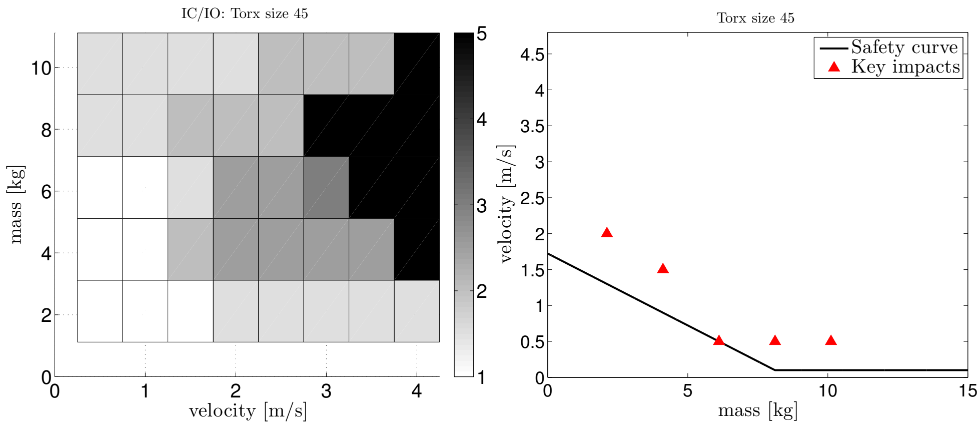

Figure 28: Risk curve (left) and safety curve (right) [12].

For safe velocity control, a threshold was defined as the maximum injury possible in terms of the AO-classification for the risk curves, in this case was IC2, i.e. contusions without skin opening. Then a new relationship velocity-mass-injury was defined, shown in Fig. 28 (right), where all the cataloged injuries for the chosen index are depicted as red triangles. Regression analysis was carried out using the risk curves and the injury data available from drop-testing. The curve that fits these injury occurrences best was shifted to the left, so that all the injuries lie above this *safety curve*. This constraining rule, then, defines the permissible velocity range for given robot's parameters, i.e. mass and velocity. It must be noted that, the velocity is limited by the injury knowledge of off-line biomechanical experiments in the form of risk and safety curves. This is a clear advantage for the control system, since no force sensor is needed in order to do this. Within ILIAD, TUM also replicated a similar drop testing setup, whereas the impact application was almost fully automated to make it easier to generate mass number of injury/safety data-sets.

4.3 Dummy crash-testing

Earlier research studies on robot-to-dummy crash-testing carried out a decade ago by the DLR [12, 26, 48, 1, 21, 44] are considered the state of the art in impact studies for physical human-robot interaction (pHRI) with lightweight and service robots. As in biomechanics and the automotive industry, the research covers impact studies with volunteers and human surrogates, i.e. animals or dummies, see Fig. 29. These studies serve as a starting point for safety evaluation in pHRI and the study of impacts in robotics. Crash-tests were carried out with the DLR/LWR, the Kuka KR6 and KR500 and against a Hybrid III Dummy at the German Automobile Club (ADAC) [44]. The experiments studied injury criteria under blunt impact to the chest, head and neck using standardized test procedures.

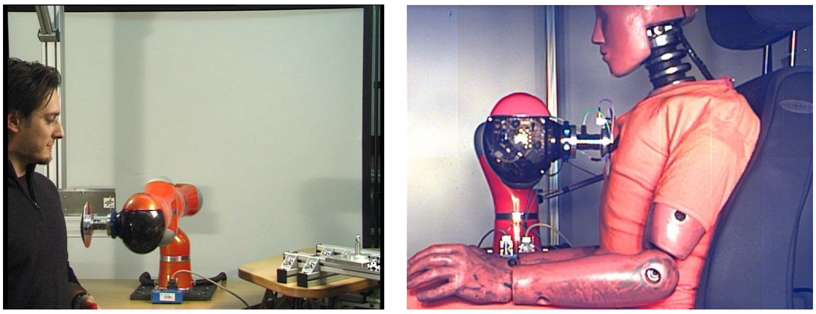

Figure 29: Blunt impact studies on human and dummy [48].

Crash tests are generally expensive and it is not possible, in general, to change parameters immediately in order to test a different impact condition, or might not be even convenient for such specific experiments. Due to all these reasons and obvious limitations for experimenting with human (cadaver) specimens, TUM has purchased a dummy and started doing further collision experiments, see Fig. 30 (left). We are currently especially interested in conducting robotic impact experiments covering the non-adequately investigated extremities. A sample arrangement in which a Franka Panda robot is configured to hit the dummy upper leg at various velocities is show in Fig. 30 (right).

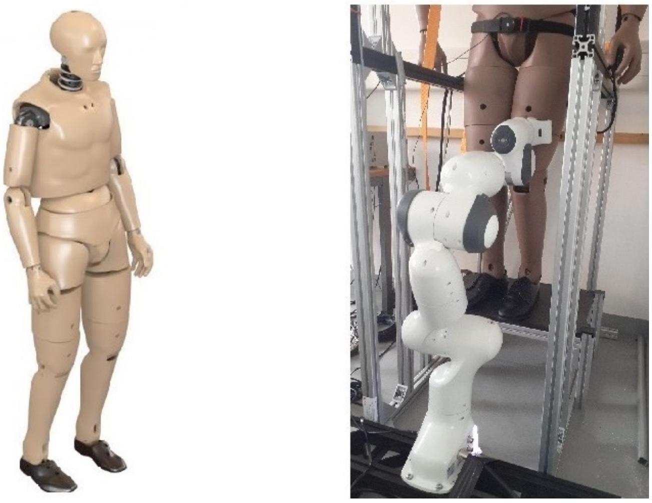

Figure 30: Robotic impact experiments with a Hybrid III 50th Male Pedestrian dummy purchased at TUM for injury biomechanics studies.

5 Safety database and relation to ISO stuff

In this section, we comment on the data-set digitization efforts and inclusion of gathered experimental impact knowledge into the safety database. We also summarize our efforts to feed the gathered valuable injury/safety data-sets into the according standardization committees on robot safety.

5.1 Safety database

In ILIAD, we extended existing literature overviews and the human injury database that we have started developing since 2012; see Fig. 31. The goal of the database is to collect all experimental impact testing and simulation data that is relevant to robotics and make this knowledge available for robot design, planning, control, and biomechanics/medical research. The database is designed such that data of arbitrary collision experiments with different setups, contact conditions, subjects, etc. can be listed and compared to each other. Furthermore, there exists convenient functions to export and analyze the stored data. We also developed the connection between the injury database and the novel Safety Map framework [49], which allows us to compare the safety characteristics of any robot system with human injury data in a unified, objective and therefore interpretation-free manner. Lastly, we added a significant amount of injury data covering various human body parts to the database. Thereby, we are making big steps towards our long term goal of thoroughly understanding the human-robot collision behavior.

5.2 Recommendations for robot safety standardization

The theoretical concepts of our proposed injury data-driven safety paradigm has largely influenced the safety standardization efforts and coined to great extents relevant international robotic standards and safety requirements such as e. g. ISO13482 for personal care robots [7] and the TS15066 for industrial robots [6]. With these we helped opening for the first time the door to HRC for stationary robots in the real industrial and service world. Continuing those successful efforts, we are continuously striving to bring safe pHRI as a reality into today's collaborative mobile robot systems and enable further breakthroughs in terms of safety certification of different autonomous industrial and service robots.

Additionally, thorough comments and recommendations were provided to the committee of the ISO/DIS 10218 draft [4, 5], the most important norm on physical human-robot interaction. Previously, many research results achieved by TUM already found their way into the norm. In our most recent comments on the ISO/DIS 10218-2 draft related to collaborative robots, we raised several important concerns that are still remaining. These are motivated by the fact that many users will rely on the new ISO standard as their main source of information about the safe and effective use of collaborative robots. The standard should provide truly the available knowledge of safe and effective human-robot collaboration. We provided recent ILIAD results to substantiate our concerns and provided recommendations to improve the norm so that a good trade-off between human safety and robot performance can be realized in collaborative robot applications. Furthermore, we offered to support the committee in this endeavor with the experience and expertise that we have gained in fundamental research on robot safety over the past two decades. A copy of the latest communication document we exchanged with the working committee on the standardization of safe collaborative robot systems summarizing our comments on the ISO/DIS 10218-2 [5] is attached in the Appendix 7. There, we raise several important concerns that are still remaining regarding information about the safe and effective use of collaborative robots. Our recent research results were provided to substantiate our concerns and provide recommendations to improve the norm, so that a good

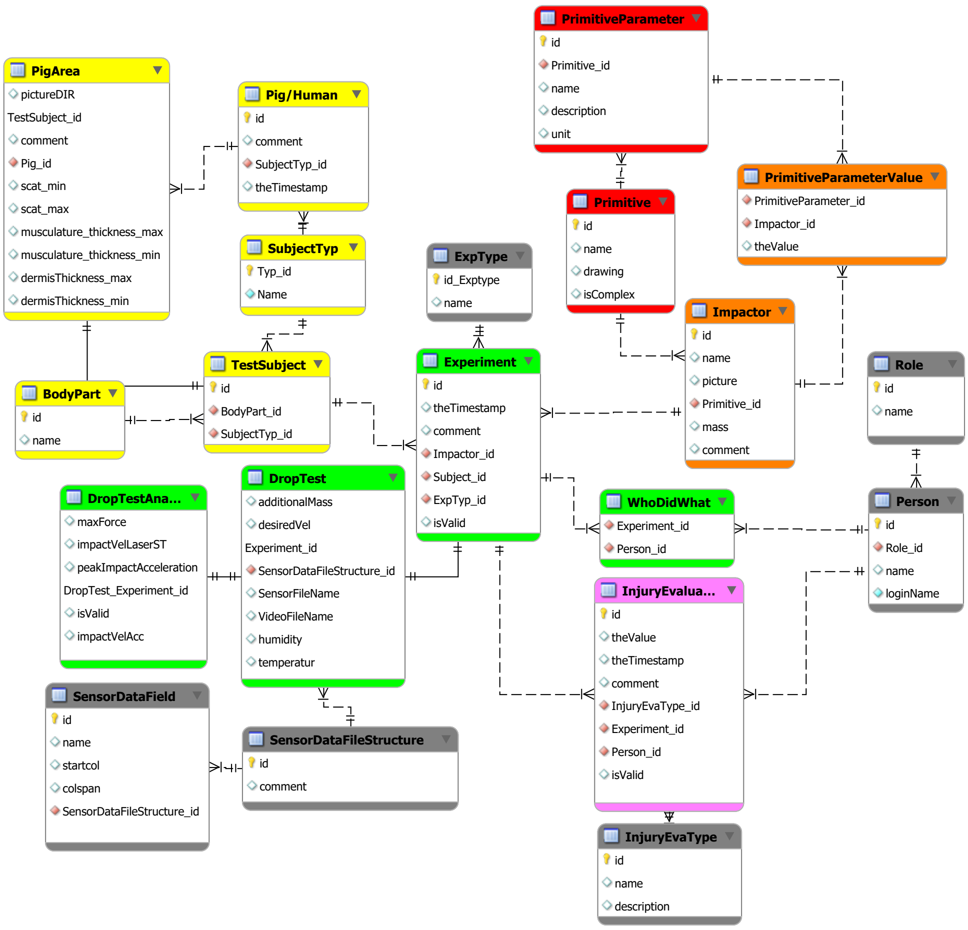

Figure 31: Entity relationship diagram of the safety database.

trade-off between human safety and robot performance can be realized in collaborative robot applications.

6 Conclusion

Following the development of more sophisticated, light-weight mechanical arm structures and agile mobile bases, together with advanced control systems, it is finally possible to eliminate classical safety barriers between the robot and human operators and enable direct interactions. The investigations in this work are motivated by the critical demand for human injury data to ensure safety of such physical human-robot interactions for autonomous robotic systems in shared workspaces. As the safety of human operators should always be guaranteed, applications that require high robot autonomy, mobility and performance are restricted by the imposed safety limits in order not to inflict injury while in direct contact with a human.

In this deliverable, we dived further into the experimental impact settings and background biomechanical knowledge around the limits of current safety standards. Our aim was to gather all reported data-sets from the published literature. To achieve this in a well-organized and comparable way, we provided meaningful abstractions for the involved experimental impact mechanisms and test setups for every human body part. Based on those, we classified and categorized the collected data-sets and further visualized them in synopsis plots summarizing the range and key trends for the findings of each experimental series. Additionally, we described different experimental set-ups we built to carry out more impact tests in order to generate the missing, required data-sets, that are relevant for robotics. All captured and generated injury/safety data-sets covering impact characterization and observed injury are being continuously fed into our digital safety database. Alongside, key insights about recommended force/torque and motion speed/acceleration tolerance limits are shared with the working groups of robotics safety standardization.

References

[1] S. Haddadin, A. Albu-Schäffer, M. Frommberger, J. Rossmann, and G. Hirzinger. The “DLR Crash Report”: Towards a standard crash-testing protocol for robot safety - part II: Discussions. In *IEEE Int. Conf. on Robotics and Automation (ICRA2008), Kobe, Japan*, pages 280–287, 2009.

[2] Lihui Wang, Sichao Liu, Hongyi Liu, and Xi Vincent Wang. Overview of Human-Robot Collaboration in Manufacturing. In *Proceedings of 5th International Conference on the Industry 4.0 Model for Advanced Manufacturing*, pages 15–58. Springer, 2020.

[3] Machinery Directive. Directive 2006/42/ec of the european parliament and of the council of 17 may 2006. *Official Journal of the European Union—09.06*, page L157, 2006.

[4] International Organization for Standardization (ISO). Robots and robotic devices - Safety requirements for industrial robots - Part 1: Robots (ISO 10218-1:2011), 2011.

[5] International Organization for Standardization (ISO). Robots and robotic devices - Safety requirements for industrial robots - Part 2: Robot systems and integration (ISO 10218-2:2011), 2011.

[6] International Organization for Standardization (ISO). Robots and robotic devices - Collaborative robots (ISO/TS 15066:2016), 2016.

[7] ISO Robots. robotic devices–safety requirements–nonmedical personal care robot. iso 13482. *International Organization for Standardization, Geneva, Switzerland*, 2014.

[8] International Standardization Organization (ISO). ISO/TR 23482-1:2020, Robotics – Application of ISO 13482 – Part 1: Safety-related test methods.

[9] International Standardization Organization (ISO). ISO/TR 23482-1:2019, Robotics – Application of ISO 13482 –Part 2: Application guidelines.

[10] Yoji Yamada, Kazutsugu Suita, H Ikeda, N Sugimoto, H Miura, and H Nakamura. Evaluation of pain tolerance based on a biomechanical method for human-robot coexistence. *Tarnsactions of JSME*, 63(612):238–243, 1997.

[11] A Muttray et al. Collaborative Robots–Determination of pain sensitivity at the human-machine-interface. *Universitatsmedizin, Institut fur Arbeits, Sozial and Umweltmedizin, Mainz. Project FP0317 Final report*, 2014.

[12] Sami Haddadin, Simon Haddadin, Augusto Khoury, Tim Rokahr, Sven Parusel, Rainer Burgkart, Antonio Bicchi, and Alin Albu-Schäffer. On making robots understand safety: Embedding injury knowledge into control. *The International Journal of Robotics Research*, 31(13):1578–1602, 2012.

[13] Borut Povse, Sami Haddadin, Rico Belder, Darko Koritnik, and Tadej Bajd. A tool for the evaluation of human lower arm injury: approach, experimental validation and application to safe robotics. *Robotica*, 34(11):2499–2515, 2016.

[14] Roland Behrens and Norbert Elkmann. Study on meaningful and verified thresholds for minimizing the consequences of human-robot collisions. In *2014 IEEE International Conference on Robotics and Automation (ICRA)*, pages 3378–3383. IEEE, 2014.

[15] Roland Behrens and Gerald Pliske. Human-Robot Collaboration: Partial Supplementary Examination [of Pain Thresholds] for Their Suitability for Inclusion in Publications of the DGUV and Standardization. *Fraunhofer IFF and Otto von Guericke University Trauma Surgery Clinic. Project FP-0430 Final report*, 2019.

[16] Carlos Faria, Ana Colim, João Cunha, João Oliveira, Nelson Costa, Paula Carneiro, Sérgio Monteiro, Estela Bicho, Luís A Rocha, and Pedro Arezes. Safety Requirements for the Design of Collaborative Robotic Workstations in Europe–A Review. In *International Conference on Applied Human Factors and Ergonomics*, pages 225–232. Springer, 2020.

[17] Sami Haddadin, Alin Albu-Schaffer, and Gerd Hirzinger. The role of the robot mass and velocity in physical human-robot interaction - part i: Non-constrained blunt impacts. In *Robotics and Automation, 2008. ICRA 2008. IEEE International Conference on*, pages 1331–1338. IEEE, May 2008.

[18] Sami Haddadin, Alin Albu-Schaffer, and Gerd Hirzinger. The role of the robot mass and velocity in physical human-robot interaction-part ii: Constrained blunt impacts. In *Robotics and Automation, 2008. ICRA 2008. IEEE International Conference on*, pages 1339–1345. IEEE, May 2008.

[19] Technical Univesrity of Munich. SMU extended for velocity shaping of nonholonomic mobile systems. Technical report, Deliverable 4.2, ILIAD project, 2019.

[20] Technical Univesrity of Munich. ^{V}SMU completed for human-safe operation of mobile autonomous systems in dynamic environments. Technical report, Deliverable 4.3, ILIAD project, 2020.

[21] Sami Haddadin, Alin Albu-Schäffer, and Gerd Hirzinger. Requirements for safe robots: Measurements, analysis and new insights. *The International Journal of Robotics Research*, 28(11-12):1507–1527, 2009.

[22] Mazin Hamad, Alexander Kurdas, Saeed Abdolshah, and Sami Haddadin. A robotics perspective on experimental injury biomechanics of human body upper extremities. In *2021 IEEE International Conference on Intelligence and Safety for Robotics (ISR)*, pages 316–320. IEEE, 2021.

[23] Kai-Uwe Schmitt, Peter F Niederer, Markus H Muser, and Felix Walz. *Trauma biomechanics: Introduction to accidental injury*. Springer Science & Business Media, 2013.

[24] JW Melvin, Richard G Snyder, LW Travis, and Nels R Olson. Response of human larynx to blunt loading. Technical report, SAE Technical Paper, 1973.

[25] Rob AC Bilo, Simon GF Robben, and Rick R Van Rijn. *Forensic aspects of pediatric fractures: differentiating accidental trauma from child abuse*. Springer Science & Business Media, 2010.

[26] Sami Haddadin, Alin Albu-Schäffer, and Gerd Hirzinger. Soft-tissue injury in robotics. In *2010 IEEE International Conference on Robotics and Automation*, pages 3426–3433. IEEE, 2010.

[27] Michael Kleinberger, Emily Sun, Rolf Eppinger, Shashi Kuppa, and Roger Saul. Development of improved injury criteria for the assessment of advanced automotive restraint systems. *NHTSA Docket*, 4405:9, 1998.

[28] Charles K Kroell, Stanley D Allen, Charles Y Warner, and Thomas R Perl. Interrelationship of velocity and chest compression in blunt thoracic impact to swine ii. *SAE transactions*, pages 649–671, 1986.

[29] John M Cavanaugh, Timothy Walilko, Jaekoo Chung, and Albert I King. Abdominal injury and response in side impact. *SAE transactions*, pages 1724–1739, 1996.

[30] Stephen W Rouhana, Stephen A Ridella, and David C Viano. The effect of limiting impact force on abdominal injury: a preliminary study. *SAE transactions*, pages 634–648, 1986.

[31] JW Melvin, Richard Lynn Stalnaker, VL Roberts, and ML Trollope. Impact injury mechanisms in abdominal organs. Technical report, SAE Technical Paper, 1973.

[32] Stephen W Rouhana. Abdominal injury prediction in lateral impact-an analysis of the biofidelity of the euro-sid abdomen. Technical report, SAE Technical Paper, 1987.

[33] Y Talantikite, F Brun-Cassan, C Tarriere, et al. Abdominal protection in side impact. injury mechanisms and protection criteria. In *Proceedings of the International Research Council on the Biomechanics of Injury conference*, volume 21, pages 131–144. International Research Council on Biomechanics of Injury, 1993.

[34] Stephen W Rouhana. Biomechanics of abdominal trauma. In *Accidental Injury*, pages 405–453. Springer, 2002.

[35] National Highway Traffic Safety Administration et al. Actions to reduce the adverse effects of airbags: Depowering, final regulatory evaluation, 1997.

[36] Charles K Kroell, Dennis C Schneider, and Alan M Nahum. Impact tolerance and response of the human thorax II. *SAE Paper No.741187, Proc. 18th Stapp Car Crash Conference, SAE Transactions*, pages 3724–3762, 1974.

[37] Lawrence M Patrick. Impact force—deflection of the human thorax. *SAE Transactions*, pages 3181–3192, 1981.

[38] D Kallieris, R Mattern, and W Härdle. Load limits and injury mechanics of the belted vehicle occupants in side impacts - phase II: Approaches to injury predictions. *FAT series of publications*, (60), 1986.

[39] Narayan Yoganandan, John Humm, Preston Greenhalgh, and Jeffrey Somers. Lower neck injury criteria for thor and hybrid iii dummies in rear impact. *Traffic injury prevention*, pages 1–3, 2020.

[40] R Cameron, D Bass, L Donnellan, R Salzar, S Lucas, B Folk, M Davis, K Rafaels, C Planchak, K Meyerhoff, et al. A new neck injury criterion in combined vertical/frontal crashes with head supported mass. In *Proceedings of the IRCOBI Conference, Madrid, Spain*, pages 20–22, 2006.

[41] S. Kirkish, P. Begeman, and N. Paravasthu. Proposed provisional reference values for the humerus for evaluation of injury potential. *40th Stapp Car Crash Conference*, (SAE 962416):1766–1775, 1996.

[42] Robin Jeanne Kirschner, Nico Mansfeld, Guillermo Gómez Peña, Saeed Abdolshah, and Sami Haddadin. Notion on the correct use of the robot effective mass in the safety context and comments on iso/ts 15066. In *2021 IEEE International Conference on Intelligence and Safety for Robotics (ISR)*, pages 6–9. IEEE, 2021.

[43] Robin Jeanne Kirschner, Nico Mansfeld, Saeed Abdolshah, and Sami Haddadin. Experimental analysis of impact forces in constrained collisions according to iso/ts 15066. In *2021 IEEE International Conference on Intelligence and Safety for Robotics (ISR)*, pages 1–5. IEEE, 2021.

[44] Sami Haddadin, Alin Albu-Schäffer, and Gerd Hirzinger. Safety evaluation of physical human-robot interaction via crash-testing. In *Robotics: Science and systems*, volume 3, pages 217–224. Citeseer, 2007.

[45] D Viano and C Warner. Thoracic impact response of live porcine subjects. paper 760823. *Society of Automotive Engineers, Warrendale, PA*, 1976.

[46] Oliver A Shergold, Norman A Fleck, and Darren Radford. The uniaxial stress versus strain response of pig skin and silicone rubber at low and high strain rates. *International Journal of Impact Engineering*, 32(9):1384–1402, 2006.

[47] S. Haddadin, A. Albu-Schäffer, and G. Hirzinger. Soft-tissue injury caused by sharp tools: Definitions, experiments and countermeasures. *IEEE Robotics and Automation Mag.*, pages 20–34, 2011.

[48] S. Haddadin, A. Albu-Schäffer, M. Frommberger, J. Rossmann, and G. Hirzinger. The “DLR Crash Report”: Towards a standard crash-testing protocol for robot safety - part I: Results. In *IEEE Int. Conf. on Robotics and Automation (ICRA2008), Kobe, Japan*, pages 272–279, 2009.

[49] Nico Mansfeld, Mazin Hamad, Marvin Becker, Antonio Gonzales Marin, and Sami Haddadin. Safety map: A unified representation for biomechanics impact data and robot instantaneous dynamic properties. *IEEE Robotics and Automation Letters*, 3(3):1880–1887, 2018.

7 Appendix: Comments on the ISO/DIS 10218-2

Comments on ISO/DIS 10218-2

Sami Haddadin[1], Matej Hoffmann[2] , Saeed Abdolshah[1], Mazin Hamad[1], Robin Jeanne Kirschner[1], Alexander Kurdas[1], Nico Mansfeld[1] and Petr Svarny[2]

[1] Technical University of Munich (TUM)
[2] Czech Technical University in Prague (CTU)

Contact: sami.haddadin@tum.de, matej.hoffmann@fel.cvut.cz

Table of contents

Introduction

We are glad to see the progress in the standardization of safe collaborative robot systems that was made within the last years and appreciate the committee's great work in putting together the latest ISO/DIS 10218-2 draft. We are glad and honored that many research results of our group found their way into the draft. In this document, we raise several important concerns that are still remaining. These are motivated by the fact that many users will rely on the new ISO standard as their main source of information about the safe and effective use of collaborative robots. The standard should provide truly the available knowledge of safe and effective human-robot collaboration. We provide recent research results to substantiate our concerns and provide recommendations to improve the norm so that a good tradeoff between human safety and robot performance can be realized in collaborative robot applications. We kindly offer to support the committee in this endeavor with the experience and expertise that we have gained in fundamental research on robot safety over the past two decades. We are willing to invest a considerable amount of time and effort to generate data, insights, and methods to address the raised concerns, even in the short term.

1. Inaccurate prediction of contact force and hazard potential due to oversimplified contact model

In annex M "Limits for quasi-static and transient contact", the considered body model, the human biomechanical force and pressure thresholds, and the relationship between the latter and transfer energy during transient contact are described. In section M.3.4, in particular table M.6, a suggestion is provided on how the robot velocity can be selected such that the threshold forces and pressures are respected during operation.

Problem

As mentioned in sections M.3.5 and M.3.6 in the draft, the considered collision model is over-simplistic and does not reflect the real contact situation. It is to be expected that the safety curves (speed vs. mass) provided in table M.6 and figure M.4 will be implemented by the majority of application engineers. However, **when implementing the specific safety curves (a concept we introduced in [1]) deduced from the model, one observes a significant mismatch between the predicted and the measured contact forces. This implies that the model is generally not suitable to draw conclusions about or to predict the hazard potential in real contact scenarios.**

This was shown in collision experiments conducted at Technical University of Munich (TUM) with a Franka Emika Panda; see Figure 1. During transient contact with a collision pressure measuring kit PRMS by Pilz GmbH, the **measured forces are up to two times higher than the forces predicted by the ISO/DIS 10218-2 model.**

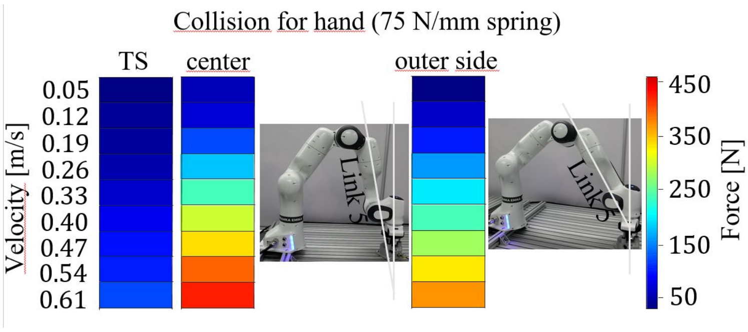

Figure 1: Transient collision experiment with Franka Emika Panda and Pilz PRMS at varying impact velocity. The robot moves vertically towards the collision test device. Two robot configurations are selected; configuration on the left and right. The color bars indicate the transient peak impact force upon contact which lasts < 0.5 seconds. On the left, the predicted forces according to ISO/DIS 10218-2 are illustrated, which are typically lower than the measured contact forces.

Furthermore, the experiments show that the contact force depends on the robot configuration; see Figure 1. In the robotics literature it is well known that the reflected mass, respectively the force/pressure or pain/injury during contact, depends on the robot configuration. However, the ISO/DIS 10218-2 does not take the dependence of robot configuration on contact force/pressure into account. The reflected robot mass is assumed to be half of the mass of the moving parts plus the payload (Eq. M.4).

For the Franka Emika Panda and KUKA Lightweight Robot IV+ (LWR) we show in Fig. 2 how the reflected mass is distributed in the robots' workspace. For the illustrated workspace grid (5 cm resolution, see [6] in the appendix for details) we evaluate the relative number of robot positions associated with a certain effective mass range; see Fig. 2 (middle, bottom). In the bar graph, we also illustrate the reflected mass obtained ISO/DIS 10218-2. For the LWR it can be observed that for approx. 60 % of the reachable workspace the reflected mass is lower than the 6.3 kg obtained by the standard. For the Panda, the reflected mass is lower than the simplified ISO estimate in 97 % of the cases. **In our experiments reported in [6] (see appendix), where we measure the reflected mass via a passive mechanical pendulum, we observe very good agreement of Khatib's reflected mass model [3] with the measured effective mass (max. 1-7 % difference for the considered robots), while there is a significant mismatch between the ISO model and the experimental results (73 - 90 % difference).**

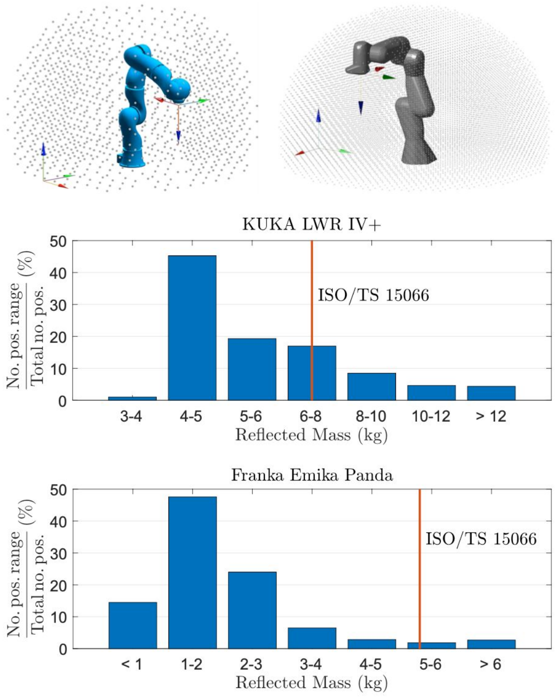

Figure 2: Cartesian positions (top) and workspace reflected mass distribution for the KUKA LWR IV+ (middle) and Franka Emika Panda (bottom). For both robots, the end-effector is pointing downwards with the end-effector frame being axis-aligned with the world coordinate frame. The reflected mass is evaluated in the downward direction.

Similar research was also presented in [5, 10] and supports the same conclusion. These data-driven approaches show that the current model in the standard both under- and over-estimates the real impact forces. Schlotzhauer presents that the reflected mass depends on the distance from the robot base in a 2D Collision Force Model (CFM) [5]. The work in [10] adds to the model also height and shows that it also significantly influences the final reflected mass. Additionally, the collected data in [10] show that the impact forces are also significantly influenced by the control mechanisms of the robots (see comparison of impact forces in Fig. 3 between the KUKA robot with various external torque settings). The current model presented in the standard does not take into account robot control properties at all (see below a separate section). A data-driven approach focused on the application allows to take these robot properties into account.

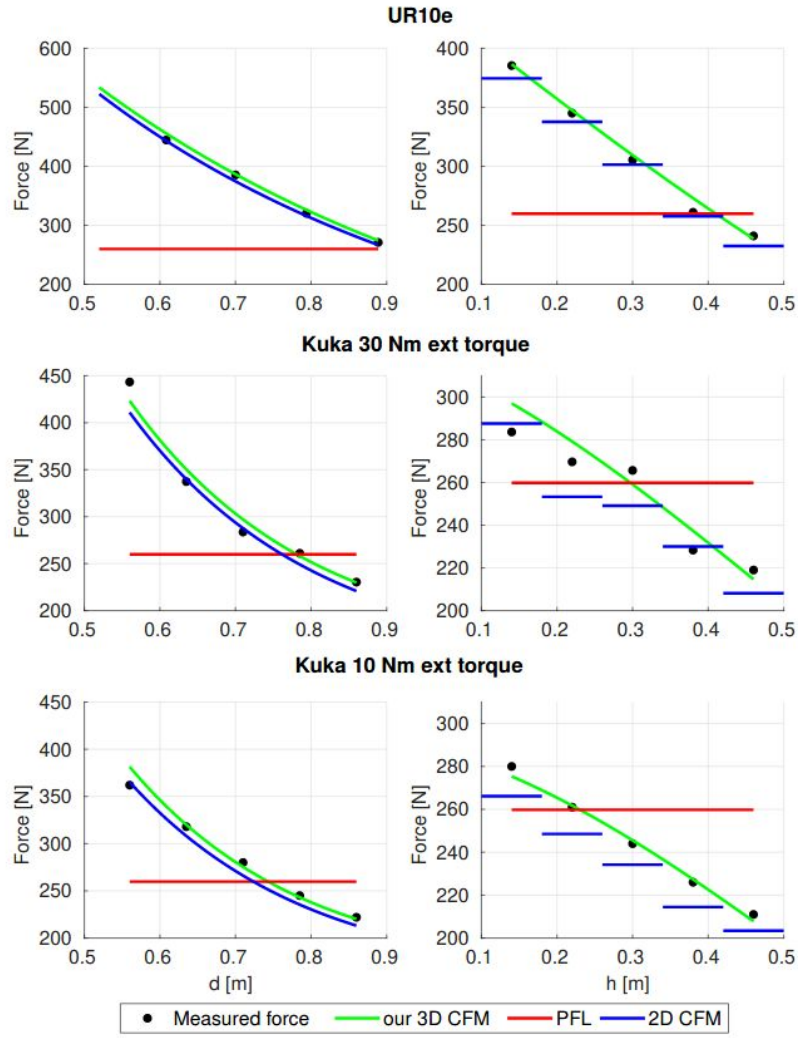

Figure 3: Impact force model comparison of two data-driven models (3D CFM [10] - green, 2D CFM [5] - blue), and the value for Power and Force Limiting (PFL) mode from the standard - red. End effector velocity = 0.30 m/s. (Top) UR10e; (Middle) KUKA with 30 Nm torque limit; (Bottom) KUKA with 10 Nm torque limit. (Left) Constant height of end effector in the workspace (0.14 m). (Right) Constant distance from base (0.70 m for UR10, 0.71 m for KUKA). Impact directions were always down, perpendicular to the table surface.

Note that the presented models all deal with top-down impacts. However, the observed effect of the robot configuration suggests that it also affects collisions that take place in other directions. The simplified contact model also does not take into account in any way the surface properties of the robot. These can be significantly altered with the use of soft protective covers. However, even analytical models that take into account surface properties, as [15], still lack detailed treatment of the manipulator control and other relevant features.

Recommendation

In general, it is difficult to model the highly non-linear contact conditions in physical human-robot interaction. **We suggest using a purely data-driven approach to relate instantaneous robot properties to injury/pain (or force/pressure), which avoids misinterpretations and simplifications.** As shown in [1] and [2], for example, the robot parameters impact velocity, configuration-dependent reflected mass [3], and contact geometry can be related to human injury/pain for realistic and a-priori model-independent safety analysis. It is also possible to relate the workspace position of a certain robot to the selected biomechanical safety criterion; cf. [5, 10].

2. Towards biomechanically safe robot velocities: Limitations of model-based over data-driven approaches

In Annex M, it is described how the robot speed can be limited to a biomechanically safe value. The biomechanical force/pressure thresholds are related to speed via a simplified collision model.

Problem

There are several problems with this approach.

1) In order to command safe robot velocities, the ISO/DIS 10218-2 approach requires a collision model. As mentioned previously and shown in literature, collisions in HRI are notoriously difficult to model. The collision model proposed in ISO/DIS 10218-2 does not capture the complex human impact behavior. Furthermore, **the approach does not enable to embed the observed pain/injury, respectively the biomechanical thresholds directly into robot control**; measurements of contact forces/pressures are indispensable in practice.

2) It is **difficult to measure quantities such as impact stress for complex geometries** (which are, however, those relevant to collaboration scenarios) even under controlled scenarios.
3) The **consistency with the medically observed injury is often insufficient** as shown in [1]. This can have multiple causes, of which the certainly most important one is that a single quantity cannot capture the complex behavior of human soft-tissue (especially in robot failure/injury cases).

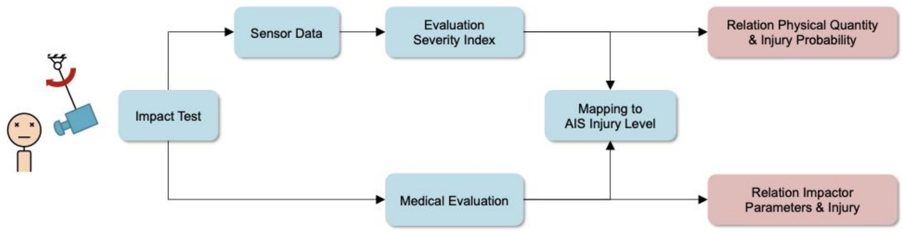

Figure 4: Comparison of model-based approaches (upper path) versus medically oriented approach (lower path) for injury analysis and prediction.

Recommendation

There exist two approaches to predict human injury/pain [1]; see Fig. 4:

1) Pain/injury prediction based on **output quantities** (ISO/DIS 10218-2)
After acquiring collision data from impact experiments (e.g., pendulum or drop tests), biomechanical analysis, medical evaluation, and statistical methods are applied to derive a relationship between measured physical output quantities such as force, deflection, or stress and resulting pain/injury; see Fig. 4 (upper path). Then threshold forces or threshold stresses (possibly nonlinear functionals) are defined. In turn, these would be used to acquire contact models and predict the resulting injury via collision simulations. This approach enables the development of anthropometric test devices, which can be used to assess the hazard potential in HRI setups.

2) Pain/injury prediction based on **input quantities:**
Instead of using an intermediate quantity such as force or pressure to relate robot parameters such as velocity, reflected mass, etc. to observed human pain/injury, the second approach uses medical observation as ‘ground truth’ and relates pain/injury probability directly to the robot input parameters; see Fig. 4 (lower path).

The **second approach has following advantages over the first approach**:

- The **safety analysis is independent of impact models, which are inherently inaccurate**.
- **No simplifications are necessary**, the medical observations by physicians serve as ground truth.
- The data-driven **relationship between collision input parameters and pain/injury can be embedded directly into planning and real-time robot control**.

A holistic solution to approach 2), i.e., from generating collision data to ensuring biomechanical safe robot trajectories via control, is described [1]. There, systematic biomechanics collision experiments were carried out to derive the **mapping between the input parameters reflected mass, velocity, contact geometry and the observed injury**. So-called safety curves were derived that provide a maximum biomechanically safe velocity as a function of instantaneous inertial robot properties. These representations were further developed into the safe velocity controller *Safe Motion Unit* that limits the instantaneous robot speed by respecting the safety curves, therefore ensuring human safety even in case of entirely unforeseen collisions.

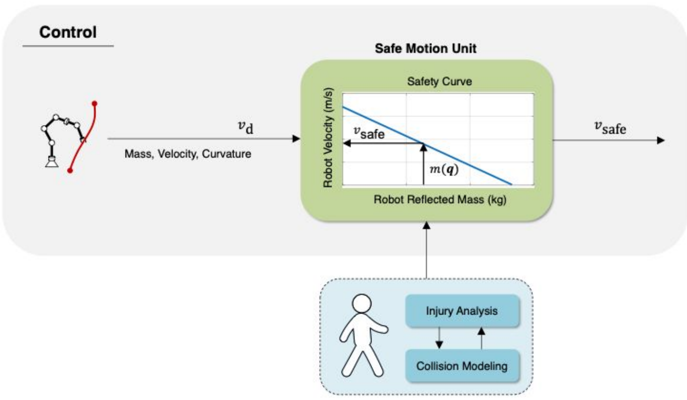

Figure 5: Safe Motion Unit [1]. Human injury data from biomechanics collision experiments or verified collision models is encoded into a safety curve, which provides the maximum biomechanically safe robot velocity given the robot's instantaneous reflected mass and contact geometry.

It is highly appreciated that our safety curve concept found its way into the ISO/DIS 10218-2, but the model-based derivation of these curves has significant limitations compared to the suggested data-driven approach. We therefore strongly encourage to rethink this concept.

3. Subjective vs. objective biomechanical thresholds

In Annex M the body model for the **onset of human pain** is provided. It is based on external force and pressure values occurring at the contact location, where the contact area is assumed to be ≥ 1 cm^2. The pain thresholds were derived within studies of the Fraunhofer IFF and the University of Mainz and included around 100 participants in total.

Problem

The problem with using pain onset (respectively pain tolerance) as a biomechanical threshold is that

a) **pain is not an objective criterion**,
b) there is a **high variance in pain onset and pain tolerance in the population**,
c) **pain strongly relies on the contact surface**, which is not accounted for in the ISO/DIS 10218-2 draft, and
d) pain thresholds may restrict the performance of HRI applications overly conservative.

In the research studies conducted in [14, 17], e.g., a **large difference in pain sensation** was observed among the participants, and consequently also in the measured contact forces. In the experiments with a flat impactor of 1 cm^2 contact area reported in [17], the margin between the upper and lower 50 th percentile was up to 300 N.

The strong reliance on the **impact surface of at least 1 cm^2** [13] (originally [61]) seems critical considering the practicability of designing robots and tools with no surface smaller than 1 cm^2 that are not rounded (as also the pain values for rounded shape were not considered fully) - note that there are trends of collaborative robots even handling welding equipment.
The results from [12] (originally [59]) show the effect of various impactor shapes and cover materials on the resulting impact pain perception. Also current research reports significantly different findings for varying contact geometries than those presented in the original research and their results show a high level of variance, see [8]. Dynamic forces of up to 300 N were still considered by the majority of test subjects in [12] as bearable as opposed to the results 140 N limit suggested in the standard.

Recommendation

In some collision scenarios such as quasi-static clamping, one can argue that pain onset is a reasonable safety criterion and certainly, HRI applications should generally be ergonomic, i.e., pain should be avoided if possible. However, due to the aforementioned limitations of pain thresholds, **we believe that the avoidance (not tolerance!) of (even minor) injury is a more**

suitable safety criterion/threshold for most collision scenarios, in particular for transient contacts with ≤ 0.5 s duration. While pain sensation is subjective and may also be influenced by the experimental protocol in clinical studies, **there exist objective, well-established classifications to assess human injury;** cf. [1]. Injury can be quantitatively assessed by physicians and **in the majority of the technical sectors where humans interact with machines, norms are concerned with injury rather than with pain.**

The suggested force/pressure thresholds for pain onset and the according robot velocities are rather restrictive, i.e., only low contact forces and velocities can be applied in PFL. **Another advantage of using injury thresholds is the possibility to enhance the performance** (cycle time) of HRI applications while ensuring safety at the same time. **This would greatly improve the acceptance and spread of collaborative robots** in start-ups, SME's, and large-scale industry.

4. Robot collision handling abilities are not considered

In both transient and quasi-static contact situations, it is important that a collaborative robot can detect and react to contacts in a safe manner. Several approaches to collision detection exist, e.g. proprioceptive (torque, current) and exteroceptive (e.g., force/torque) sensing [16].

Problem

The current ISO/DIS 10218-2 draft does not consider the collision handling capabilities of collaborative robots, i.e., requirements and methods to assess the collision detection, reaction and control performance upon contact are not defined. **However, in HRI applications this information is very important to vastly improve the user's safety and maximize injury prevention for protection**, as he/she needs to know whether his/her robot is capable of detecting and reacting to possibly hazardous contact.

Recommendation

We are currently developing a standardized benchmark test to assess the collision handling capabilities of robot systems. The benchmark considers all relevant parameters that influence the contact sensitivity. The outcome is a tool that can be easily and quickly integrated into the planning and execution phase of HRI applications. A publication on this benchmark test is currently under review. For further information please contact us.

5. Typos and other minor comments

Line	Sec.	Fig/Tab/Eq	Comment
3909, 3910	M.4	Fig M.5	The figure is accompanied by two different captions. Most probably Figure M.5 is missing.
3909, 3910	M.4	Fig M.5	It seems that a polynomial function was used to fit the data provided in Table M.6 and that the curves were not derived via equations M.1 - M.6.
3993	N.1.5	Table N.1	The table is unreferenced, it would be good to know where those values come from.
3867	M.4	Table M.4	The table is unreferenced, it would be good to know where those values come from.
3906	M.3.4.1	Table M.6	The table lacks an understandable naming. We assume 1,2,3,5,10,15,20 are supposed to be different values for the robot effective mass, while the numbers inside the table are velocities.

Please note that Sami Haddadin has a potential conflict of interest as shareholder of Franka Emika GmbH.

References

[1] Haddadin S, Haddadin S, Khoury A, et al. On making robots understand safety: Embedding injury knowledge into control. The International Journal of Robotics Research. 2012;31(13):1578-1602.

[2] Mansfeld, N., Hamad, M., Becker, M., Marin, A. G., & Haddadin, S. (2018). Safety map: A unified representation for biomechanics impact data and robot instantaneous dynamic properties. IEEE Robotics and Automation Letters, 3(3), 1880-1887.

[3] Khatib, O. (1987). A unified approach for motion and force control of robot manipulators: The operational space formulation. IEEE Journal on Robotics and Automation, 3(1), 43-53.

[4] Kirschner, R.J., Mansfeld, N., Abdolshah, S., and Haddadin, S.: Experimental Analysis of Impact Forces in Constrained Collisions According to ISO/TS 15066, IEEE International Conference on Intelligence and Safety for Robotics, 2021 (accepted).

[5] Schlotzhauer, A., Kaiser, L., Wachter, J., Brandstötter, M., & Hofbaur, M. On the trustability of the safety measures of collaborative robots: 2D Collision-force-map of a sensitive manipulator for safe HRC. In 2019 IEEE 15th International Conference on Automation Science and Engineering (CASE) (pp. 1676-1683).

[6] Kirschner, R.J., Mansfeld, N., Gomez, G., Abdolshah, S., and Haddadin, S.: Notion on the Correct Use of the Robot Effective Mass in the Safety Context and Comments on ISO/TS 15066, IEEE International Conference on Intelligence and Safety for Robotics, 2021 (accepted).

[7] Weitschat, R., Ehrensperger, J., Maier M., and Aschemann H., "Safe and Efficient Human-Robot Collaboration Part I: Estimation of Human Arm Motions," 2018 IEEE International Conference on Robotics and Automation (ICRA), Brisbane, QLD, 2018, pp. 1993-1999, doi: 10.1109/ICRA.2018.8461190.

[8] Park, M. Y., Han, D., Lim, J. H., Shin, M. K., Han, Y. R., Kim, D. H., ... & Kim, K. S. (2019). Assessment of pressure pain thresholds in collisions with collaborative robots. *PloS one*, *14*(5), e0215890.

[9] Han, D., Park, M. Y., Shin, H., Kim, K. S., & Rhim, S. (2018, June). Identifying Safety Conditions of Human-Robot Collision based on Skin Injury Analysis. In *2018 15th International Conference on Ubiquitous Robots (UR)* (pp. 420-423). IEEE.

[10] Svarny, P., Rozlivek, J., Rustler, L., & Hoffmann, M. (2020). 3D Collision-Force-Map for Safe Human-Robot Collaboration. (under review) Available: arXiv preprint arXiv:2009.01036.

[11] Haddadin S, Albu-Schäffer A, Hirzinger G. Requirements for Safe Robots: Measurements, Analysis and New Insights. The International Journal of Robotics Research. 2009; 28(11-12): 1507-1527.

[12] Mewes, D. and F. Mauser: “Safeguarding Crushing Points by Limitation of Forces.” International Journal of Occupational Safety and Ergonomics. 2003, 9. (2): 177-191.

[13] Research project No. FP-0317: Collaborative robots – Investigation of pain sensibility at the Man-Machine-Interface. Institute for Occupational, Social and Environmental Medicine at the Johannes Gutenberg University of Mainz, Germany. Final report December 2014

[14] Yamada, Y., & Sugimoto, N. (1995). Evaluation of human pain tolerance. Journal of the Robotics Society of Japan, 13(5), 639-642.

[15] Vemula, B., Matthias, B., & Ahmad, A. (2018). A design metric for safety assessment of industrial robot design suitable for power-and force-limited collaborative operation. *International journal of intelligent robotics and applications*, *2*(2), 226-234.

[16] Haddadin, S., De Luca, A., & Albu-Schäffer, A. (2017). Robot collisions: A survey on detection, isolation, and identification. IEEE Transactions on Robotics, 33(6), 1292-1312.

[17] Behrens, Roland. Biomechanische Grenzwerte für die sichere Mensch-Roboter-Kollaboration. Springer Vieweg, 2019.

Experimental Analysis of Impact Forces in Constrained Collisions According to ISO/TS 15066

Robin Jeanne Kirschner[1], Nico Mansfeld, Saeed Abdolshah and Sami Haddadin

***Abstract*— For the user of a collaborative robot, it is important to select robot parameters and trajectories such that the task is fulfilled while ensuring human safety at the same time. In human robot interaction (HRI), constrained collisions can be particularly hazardous to the human and recently, collision test devices were developed that assess safety in such scenarios. In this paper, we propose the concept of a constrained collision force map (CCFM), which relates the robot impact velocity and the collision reaction method its parameterization to the peak collision force in a constrained collision scenario. The CCFM is a tool that will help practitioners to implement both safe and efficient HRI applications and to understand the robot's collision behavior. In this work, we derive the CCFM for three robots (UR10e, UR5e, and Franka Emika Panda) for varying contact thresholds, contact stiffnesses, and robot poses. Finally, we compare our results with the force estimation suggested by ISO/TS 15066:2016.**

I. INTRODUCTION

As the demand for HRI increases, it has become paramount to analyze the performance of different lightweight collaborative robots for their validation and for designing or selecting the most appropriate system for certain tasks. Well known performance metrics like pose repeatability, maximum reach, and payload should be extended by the robot's inherent safety characteristics as they are important for modern collaborative robots [1], [2], [3]. Such safety characteristics should consider human injury probability during contact [4], [6] and the robot's collision sensing and handling capabilities [5]. The current technical specification for safe HRI, ISO/TS 15066:2016 (ISO/TS) specifies that human pain onset (in particular in constrained contact settings) shall be avoided by limiting the contact force. The contact force in HRI depends on several factors, e.g., the robot speed, configuration, inertial, and surface properties, and the collision detection and reaction methods. There exist many methods to detect and identify collisions, which either rely on proprioceptive (motor current, joint torque) or exteroceptive robot measurements. An overview of common collision detection schemes is provided in [7].

For the robot user, it is difficult to predict or model contact forces in HRI. In this paper, we introduce the concept of constrained collision force maps (CCFM). A CCFM quantifies a robot's contact sensitivity in constrained contact scenarios depending on the collision detection parameters and the robot impact velocity. It is a practical tool that enables the user to understand the robot's impact behavior and to estimate the potential hazard during impacts. We experimentally derive the CCFM for three different robots, namely the Universal Robot's (UR) UR10e, UR5e, and the Franka Emika (FE) Panda, where we analyze the influence of collision thresholds, collision stiffnesses, and robot poses on the resulting peak impact force measured by a Pilz PRMS collision test device.

This paper is structured as follow. Section II gives an overview of collisions in physical HRI and possible benchmark tests. In Sec. III we introduce the idea of CCFMs. In Sec. IV-A and IV-B the experimental results of the considered robots are presented and force and torque thresholds are compared. Finally, Sec. V concludes the paper.

II. COLLISION BENCHMARKING IN HRI

To supply general performance benchmarks of industrial robots like repeatability and accuracy the standard ISO 9283:1998 was launched [8]. It defines a cube of reference positions applicable to every robot system. This cube is based on the robot minimum and maximum reach and shall be defined as typical operating workspace. ISO 9283:1998 provides guidelines how to apply this cube to obtain general performance metrics like pose repeatability. Benchmarks for motion planning are suggested in [9], which base on the user-experience. In [10] a collection of applied context dependent performance metrics for pHRI is presented. In the context of perception, authors mention applying metrics based on the signal detection and classification accuracy and describe those by success rate of recognition. Recently, collaborative robots task performance measurement is discussed and a standardized approach is introduced [11].

Obviously, also evaluating collision handling schemes requires experimental observation [7]. For robot safety based on ISO/TS [1] testing devices for collision forces were used to test robots compliance to safety [5]. Nevertheless, still no standardized procedure to evaluate the performance of collision reaction schemes especially according to their qualification on real systems is known to the authors. Therefore, we propose to use the existing devices for safety evaluation of collisions in HRI to generate a benchmark.

III. CCFM FOR BENCHMARKING CONSTRAINED COLLISIONS

A. Collision test device

The technical specification ISO/TS 15066:2016 [1] introduces a model of the human body, which covers 21 body regions. For each body region, a contact stiffness and a pain tolerance is provided. The hand thresholds of the body model are exemplary depicted in Fig. 1. These thresholds were derived in constrained contact situations, where the human body part was attached to a rigid surface for repeatable

[1]Authors are with Institute for Robotics and System Intelligence, Munich School of Robotics and Machine Intelligence, Technical University of Munich, 80797 Munich, Germany robin-jeanne.kirschner@tum.de

measurements [12]. We use the collision pressure measuring kit PRMS by company Pilz, to obtain forces curves and peak impact forces. It consists of a one-dimensional load cell, a spring, and a rubber cover. Multiple springs and three covers are available to adapt the stiffness according to the stiffness of the considered human body part.

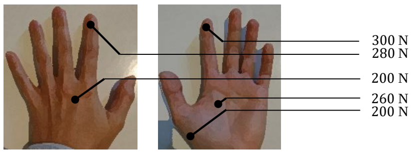

Fig. 1. Force thresholds for quasistatic contact on the dominant hand for HRI regarding to the bodymodel in ISO/TS [1].

B. Experimental design for deriving CCFMs

Using the PRMS force measurement set we investigate for the CCFMs by observing collision forces occurring during collisions using the most sensitive robot settings for UR10e, UR5e and FE Panda. As the human hand occurs to be the body part, which is most likely to be involved in a constrained collision we initially focus our assessment on a human hand model. We use a spring with constant $c = 75\,\mathrm{N/mm}$ and a cover with $70\,\mathrm{ShA}$ for the human hand. The force threshold for transient contact given by the PRMS device in accordance to ISO/TS is $280\,\mathrm{N}$ and the quasi-static threshold is $120\,\mathrm{N}$. To define a comparable position for the collision we defined each robot's reference cube according to DIN EN ISO 9283 [8]. The PRMS device is mounted to the table as shown in Fig.2 and we use a Cartesian motion generator to collide with the PRMS device at a desired speed. Due to the maximum permissible collision force of $500\,\mathrm{N}$ for the PRMS device we start with $0.05\,\mathrm{m/s}$ and stop at $0.61\,\mathrm{m/s}$.

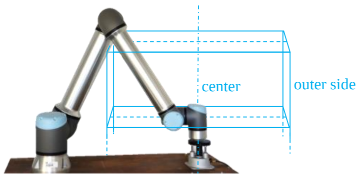

Fig. 2. Experimental setup based on the reference cube and the PRMS collision test device for evaluating the constrained contact sensitivity of a robot demonstrated by a UR10e robot.

Using the generated data, we establish the CCFMs, which depict the peak force occurring at a collision depending on the collision threshold and contact velocity. This peak impact force is inherently related to the reactiveness of the robot and may exceed the defined collision thresholds. As most robots are capable to provide collision force thresholds of $100\,\mathrm{N}$, we designed the map to consider force thresholds up to $100\,\mathrm{N}$ maximum. Nevertheless, some tactile robots provide also torque limitation, which may lead to more sensitive reaction schemes. We, therefore, investigate if the torque limitation decreases the peak collision forces compared to the force limitation. Due to the mass-force relation we include an analysis of different positions for collision and additionally observe the effect of low contact stiffness on the peak impact force.

C. The influence of collision reaction

The robot's collision reaction can contribute to the impulse transferred at a collision. Following, we therefore look at the implemented collision reaction of UR and FE Panda. At collision, the UR robots show a retracting motion depicted in Fig. 3. During the collision, the motion of the UR is reversed and the constrained contact released.

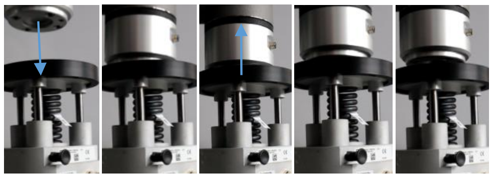

Fig. 3. Retracting motion of UR robots at collision.

The FE Panda's collision reaction relies on its compliance. Instead of triggering a backwards motion, it stops and due to its low joint stiffness the force on the contact is released as shown in Fig. 4.

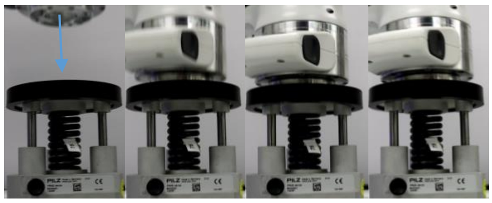

Fig. 4. Braking motion of FE Panda at collision.

IV. Peak Impact Forces as Measure of CCFMs

A. UR robots

The UR robots both enable to set the safety thresholds for collision to $F_{\mathrm{max}} = 100\,\mathrm{N}$. Therefore, we observe the peak forces occurring during the constrained collision using this setting. Fig. 5 and 6 depict the force curves derived with velocities between $0.05\,\mathrm{m/s}$ and $0.54\,\mathrm{m/s}$. For the UR10e and UR5e of collisions notice that according to ISO/TS 15066:2016 the thresholds for transient contact with a human hand are fulfilled below $0.26\,\mathrm{m/s}$. Surprisingly, the results for UR5e with velocities above $0.4\,\mathrm{m/s}$ show a second increase in force at around $400\,\mathrm{ms}$. We assume this is a result of the collision reaction mechanism.

To obtain the CCFMs in Fig. 7 and Fig. 8 we map the recorded maximum peak forces to the collision constraint setting and the applied collision velocity.

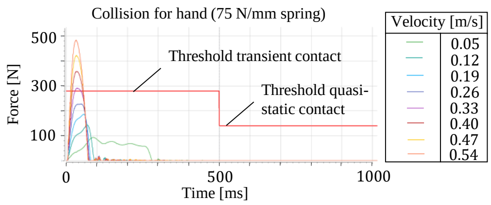

Fig. 5. Force over time measured with the PRMS device of the UR10e.

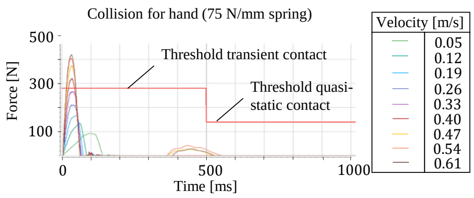

Fig. 6. Force over time measured with the PRMS device of the UR5e.

B. Franka Emika Panda

Similar experiments are conducted with the FE Panda. The force curve for the threshold $100\,\mathrm{N}$ is depicted by Fig. 10. Besides the threshold $100\,\mathrm{N}$ FE Panda allows to set lower force thresholds from which we obtain the following CCFM in Fig. 9.

For comparison of applying joint torque thresholds instead of end effector force thresholds, we investigate the most sensitive torque threshold, which is applicable using our motion generator (Cartesian fourth order) and derive the peak impact forces.

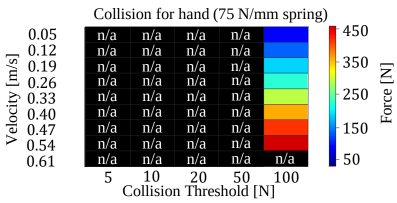

Fig. 7. CCFM of UR10e with maximum contact sensitivity settings $100\,\mathrm{N}$.

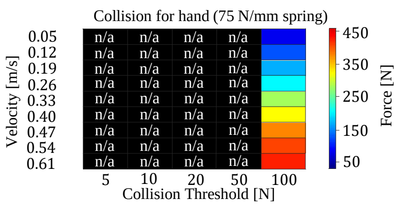

Fig. 8. CCFM of UR5e with maximum contact sensitivity setting $100\,\mathrm{N}$.

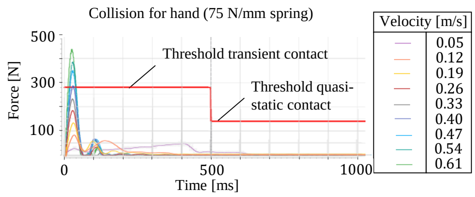

Fig. 9. Force over time measured with the PRMS device of the FE Panda.

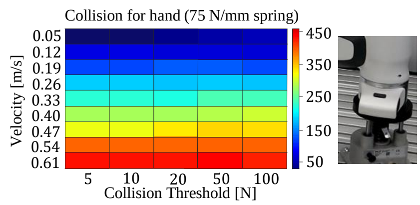

Fig. 10. CCFM of FE Panda with various contact sensitivity settings.

C. Effect of collision thresholds on peak impact force

With these experiments, we find that setting the collision thresholds hardly influences the maximum force measured by the PRMS device. It can be observed that using thresholds below $F_{\max} = 20\,\mathrm{N}$ decreases the peak impact force in contacts with low velocities like $0.05\,\mathrm{m/s}$. As already reported in [13], the application of collision reaction schemes appears to be unable to mitigate the occurring peak impact forces. As we can see from Fig. 9 and 11 the time, in which the impact force builds up within the first approx. $5\,\mathrm{ms}$ resulting in an even shorter time frame for collision detection and reaction. We conclude that with the PRMS device using the $75\,\mathrm{N/mm}$ spring an almost rigid contact occurs leaving few time for improving the collision force by collision reaction and detection. UR5e and FE Panda only differ slightly considering the occurring peak forces while the UR10e, which has a higher mass causes significantly higher forces, suggesting that differing results between FE Panda and both UR robots are based on the robots' masses. Therefore, major changes of the effective mass are expected considering different points inside the robot workspace.

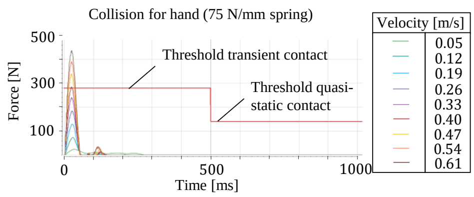

Fig. 11. Forces curves for collisions with threshold $[2.5, 2.5, 2.0, 2.0, 1.5, 1.5, 1.0]$ Nm measured with the PRMS device of the FE Panda

D. *Effect of contact stiffness on peak impact force*

The influence of the spring stiffness and the material stiffness on the robots collision performance becomes visible, when equipping the CCFM for a collision with an abdominal muscle in comparison to the CCFMs derived for the human hand in Section IV-B. The model of the abdominal muscle consists of a spring $c = 10\,\mathrm{N/mm}$ and a covering material with $10\,\mathrm{ShA}$, shown in Fig. 12. The more flexible contact seemingly decelerates the increase of the force at the collision and enables the robots sensing systems and controller to react sooner. This leads to a visible effect of using lower collision thresholds on the peak forces occurring during the collision. At velocity $0.05\,\mathrm{m/s}$ and $5\,\mathrm{N}$ and $10\,\mathrm{N}$ the peak impact force is not detected by the sensor integrated to the PRMS device.

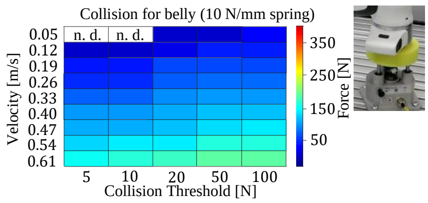

Fig. 12. CCFM for FE Panda at collisions with the abdominal muscle with spring constant $c = 10\,\mathrm{N/mm}$ and covering material with $10\,\mathrm{ShA}$.

E. *Effect of robot pose on peak impact force*

Next, we consider two different positions for the collision; at the centre of the reference cube and $-5\,\mathrm{cm}$ from its outer side. We obtain lower peak forces at the outer edge, which can be explained by the orientation of the robot's link 5 depicted in Fig. 13. At the first collision point it is almost vertical while at the second it is tilted about $45°$ to the ground. Therefore, less of its mass contributed to the occurring impact force. Generally, the results in Fig. 13 named center and outer side demonstrate that the effective mass and, therefore, the pose of the robot influences the peak impact force.

F. *Comparison to force estimation using ISO/TS 15066*

Based on Sec. IV-E we evaluated the difference in force predicted by the collision model in ISO/TS 15066:2016 and our measurements. The maximum contact force according to the model is

$$F_{\mathrm{col}} = v_{rel}\sqrt{\mu k}\,, \tag{1}$$

where k is the contact stiffness of the body part (human hand ($k = 75\,\mathrm{N/mm}$) in our experiment), v_{rel} the relative velocity, and μ the effective mass between human and robot [1]

$$\mu = \left(\frac{1}{m_{\mathrm{r}}} + \frac{1}{m_{\mathrm{h}}}\right)^{-1}. \tag{2}$$

The human mass is m_{h} (for the human hand $m_{\mathrm{h}} = 0.6\,\mathrm{kg}$) and the robot mass is

$$m_{\mathrm{r}} = M/2 + m_{\mathrm{L}}\,, \tag{3}$$

where the total mass of all moving links is denoted by M, and the load m_{L} [1]. For each considered velocity we calculate the estimated force based on ISO/TS 15066:2016 and compare these values to our previous results in Fig. 13. For each impact we observe a significant underestimation in contact force.

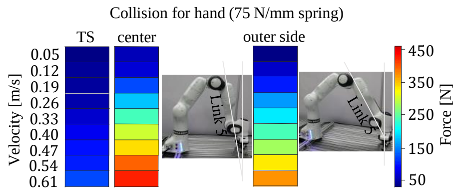

Fig. 13. CCFM for FE Panda with 100N threshold at outer side and centre of the reference cube compared to the results for estimating the force by ISO/TS 15066 (TS).

V. Discussion and Conclusion

In this paper, we introduced constrained collision force maps (CCFMs) as a benchmark for evaluating the collision behavior of collaborative robots in constrained collision scenarios. The CCFM is a practical tool that helps the user to implement safe robot applications and understand the collision behavior of his/her robot. We experimentally derived the CCFM for the UR10e, UR5e, and the Franka Emika Panda using different collision velocities and robot collision detection thresholds. Additionally, we investigated the difference in contact sensitivity between torque- and force-based collision thresholds. In terms of the absolute value of the collision thresholds, no noticeable influence on resulting peak contact forces was observed when using a high contact stiffness. Considering lower contact stiffness, however, the collision detection thresholds do influence the peak collision force. The varying peak impact forces among the three robots observed for high contact stiffness can most likely be explained by the significantly different inertial properties. Lastly, a comparison between our measurements and the collision force model in ISO/TS 15066:2016 showed large differences, which implies that the ISO/TS model is not well suited for estimating collision forces. The derivation of the CCFM for further robot workspace locations and the analysis of additional robots like the KUKA iiwa or the Techman TM5 is subject to future work.

Acknowledgment

The authors would like to thank Joao Jantalia for helping with conducting the experiments. We gratefully acknowledge the funding of the Lighthouse Initiative Geriatronics by StMWi Bayern (Project X, grant no. 5140951) and LongLeif GaPa gGmbH (Project Y, grant no. 5140953), the European Union's Horizon 2020 research and innovation program as part of the project ILIAD under grant no. 732737 and the support by the European Union's Horizon 2020 research and innovation program as part of the project I.AM. under grant no. 871899. Please note that S. Haddadin has a potential conflict of interest as shareholder of Franka Emika GmbH.

REFERENCES

[1] ISO/TS 15066:2017, *Robots and robotic devices - Collaborative robots*, Beuth-Verlag, Berlin.

[2] V. Bhanoday, B Matthias, A. Ahmad. "A design metric for safety assessment of industrial robot design suitable for power-and force-limited collaborative operation." International journal of intelligent robotics and applications 2.2 (2018): 226-234.

[3] D. Kirschner, A. Schlotzhauer, M. Brandstötter, M. Hofbaur, "Validation of Relevant Parameters of Sensitive Manipulators for Human-Robot Collaboration," in Advances in Service and Industrial Robotics, RAAD 2017, Mechanisms and Machine Science, 2018, vol 49. Springer, Cham.

[4] S. Haddadin, S. Haddadin, A. Khoury, T. Rokahr, S. Parusel, R. Burgkart, A. Albu-Schäffer, "On making robots understand safety: Embedding injury knowledge into control", *The International Journal of Robotics Research*, vol. 31, 13th ed, 2012, pp. 1578?1602.

[5] A. Schlotzhauer, L. Kaiser, J. Wachter, M. Brandstötter and M. Hofbaur, "On the trustability of the safety measures of collaborative robots: 2D Collision-force-map of a sensitive manipulator for safe HRC," 2019 IEEE 15th International Conference on Automation Science and Engineering (CASE), Vancouver, BC, Canada, 2019, pp. 1676-1683.

[6] N. Mansfeld, M. Hamad, M. Becker, A. G. Marin and S. Haddadin, "Safety Map: A Unified Representation for Biomechanics Impact Data and Robot Instantaneous Dynamic Properties," in IEEE Robotics and Automation Letters, vol. 3, no. 3, pp. 1880-1887, July 2018.

[7] S. Haddadin, A. De Luca and A. Albu-Schäffer, "Robot Collisions: A Survey on Detection, Isolation, and Identification," in IEEE Transactions on Robotics, vol. 33, no. 6, pp. 1292-1312, Dec. 2017.

[8] ISO 9283:1998, *Manipulating industrial robots - Performance criteria and related test methods*, Beuth Verlag, Berlin.

[9] B. Cohen, I. A. Şucan and S. Chitta, "A generic infrastructure for benchmarking motion planners," 2012 IEEE/RSJ International Conference on Intelligent Robots and Systems, Vilamoura, 2012, pp. 589-595.

[10] A. Steinfeld, et al. "Common metrics for human-robot interaction," 2006 1st ACM SIGCHI/SIGART conference on Human-robot interaction (HRI '06), New York, NY, USA, 2006. 33-40.

[11] K. Kimble, K. Van Wyk, J. Falco, E. Messina, Y. Sun, M. Shibata, W. Uemura, and Y. Yokokohji, Benchmarking Protocols for Evaluating Small Parts Robotic Assembly Systems, IEEE Robotics and Automation Letters, vol. 5, no. 2, pp. 883-889, 2020.

[12] R. Behrens, "Biomechanische Grenzwerte für die sichere Mensch-Roboter-Kollaboration." Springer Vieweg, in Springer Fachmedien Wiesbaden GmbH, 2019.

[13] S. Haddadin, A. Albu-Schffer, and G. Hirzinger. "Dummy crash-tests for the evaluation of rigid human-robot impacts." International Workshop on Technical Challenges for dependable robots in Human Environments. 2007.

Notion on the Correct Use of the Robot Effective Mass in the Safety Context and Comments on ISO/TS 15066

Robin Jeanne Kirschner, Nico Mansfeld, Guillermo Gómez Peña, Saeed Abdolshah and Sami Haddadin

***Abstract*— Collision experiments in the human-robot interaction (HRI) context showed that the effective robot mass is one of the main parameters that influence human injury probability during a collision. Also the current standard ISO/TS 15066 highlights the importance of this parameter and provides a method to determine the maximum safe robot velocity based on the effective mass. To enable both safe and efficient robot applications, it is crucial to derive the robot's instantaneous effective mass sufficiently accurate based on either a), a kinematic and dynamic model or b), a suitable collision experiment. In this paper, we describe and quantitatively compare the well-established reflected mass model by Khatib and the simplified model provided in the ISO/TS 15066 for the KUKA LWR IV+ and the Franka Emika Panda robot. Furthermore, we propose a method to practically determine the effective mass using a passive mechanical pendulum setup. Our results show that the simplified ISO/TS model can lead to a significant safety-relevant error. With our preliminary experimental setup, however, we can verify that the reflected mass obtained by the dynamics model only differs $1.1-7.8\,\%$ from the measured value.**

I. INTRODUCTION

A primary concern in human-robot interaction (HRI) is to ensure human safety even in dynamic, partially unknown environments. Many efforts have been taken to understand the collision dynamics in different contact scenarios [1], [2], [3]. The human injury probability during a collision is influenced by several robot parameters, e.g., the robot kinematic and inertial properties, the impact velocity, the surface properties (blunt/edgy, rigid/elastic, etc.), and the joint/link stiffness [4], [6]. In [10], [5], comprehensive collision experiments were conducted with crash-test dummies and soft tissue, where the role of the robot's reflected mass [8], i.e., the mass perceived during a collision, and velocity was investigated. In [10], the data-driven relation *(reflected mass, velocity, contact curvature)* $\rightarrow$ *injury* was established and systematic biomechanical impact experiments were carried out. So-called safety curves were derived from the experimental results, which relate the instantaneous robot reflected mass and contact geometry to a biomechanically safe velocity, which can be commanded to the robot. Such safety curves are also included in the current standard ISO/TS 15066:2016 (ISO/TS). In the norm, the robot reflected mass and endpoint velocity are related to the maximum estimated collision force via a simplified collision model. The reflected mass is calculated with a simplified model which differs from [8]. In order to successfully implement the safety curves provided in

The authors are with Institute for Robotics and System Intelligence, Munich School of Robotics and Machine Intelligence, Technical University of Munich, 80797 Munich, Germany robin-jeanne.kirschner@tum.de

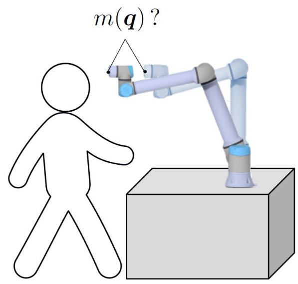

Fig. 1. The robot effective mass is a crucial parameter for safety assessment and safe control in HRI.

the ISO/TS, respectively [10], it is important to determine the robot's reflected mass sufficiently accurate, as an incorrect reflected mass can deteriorate both the human safety and performance of the system. In this paper we

- investigate the workspace effective mass distribution based on the well-established model [8] and the simplified ISO/TS model for the KUKA LWR IV+ and the Franka Emika Panda,
- conduct an experiment to derive the effective mass by observing the impulse received by an object, and
- draw implications on human safety and robot efficiency in HRI from our simulated and real-world results.

This paper is structured as follows. In Sec. II, we summarize methods to determine the reflected robot mass. For the two considered robots, we derive the workspace mass distribution in Sec. III. The experimental derivation of the reflected mass is considered in Sec. IV, implications on safe velocity control are given in Sec. IV-C. Finally, Sec. V concludes the paper.

II. EFFECTIVE MASS IN THE SAFETY CONTEXT

The robot effective mass (also referred to as the reflected mass or inertia) is the mass that an object or the human perceives during a collision. It depends on the robot's kinematic and inertial properties, the joint configuration, the joint, link, and contact elasticity as well as possibly the controller.

Consider the link side robot dynamics

$$\boldsymbol{M}(\boldsymbol{q})\ddot{\boldsymbol{q}} + \boldsymbol{C}(\boldsymbol{q},\dot{\boldsymbol{q}})\dot{\boldsymbol{q}} + \boldsymbol{g}(\boldsymbol{q}) = \boldsymbol{\tau} + \boldsymbol{\tau}_{\mathrm{ext}}\,, \tag{1}$$

where the joint and external torque are expressed as $\boldsymbol{\tau} \in \mathbb{R}^n$ and $\boldsymbol{\tau}_{\mathrm{ext}} \in \mathbb{R}^n$ and the robot's link positions and velocities are denoted $\boldsymbol{q} \in \mathbb{R}^n$ and $\dot{\boldsymbol{q}} \in \mathbb{R}^n$. The symmetric, positive definite inertia matrix is $\boldsymbol{M}(\boldsymbol{q}) \in \mathbb{R}^{n\times n}$, the Coriolis matrix is $\boldsymbol{C}(\boldsymbol{q},\dot{\boldsymbol{q}}) \in \mathbb{R}^{n\times n}$, and the gravity vector is $\boldsymbol{g}(\boldsymbol{q}) \in \mathbb{R}^{n}$. The reflected mass perceived at the point of contact in the Cartesian unit direction of impact $\boldsymbol{u} \in \mathbb{R}^3$ is given by [8]

$$m_{\mathrm{r}} = \left(\boldsymbol{u}^{\mathsf{T}} \boldsymbol{\Lambda}_{\nu}^{-1}(\boldsymbol{q})\boldsymbol{u}\right)^{-1}, \tag{2}$$

where $\boldsymbol{\Lambda}_{\nu}^{-1}(\boldsymbol{q})$ is the upper 3×3 matrix of the robot Cartesian mass matrix inverse

$$\boldsymbol{\Lambda}(\boldsymbol{q})^{-1} = \boldsymbol{J}(\boldsymbol{q})\boldsymbol{M}(\boldsymbol{q})\boldsymbol{J}(\boldsymbol{q})^{\mathsf{T}}, \tag{3}$$

with $\boldsymbol{J}(\boldsymbol{q}) \in \mathbb{R}^{n\times m}$ being the Jacobian matrix at the point of contact. For rigid robots $\boldsymbol{M}(\boldsymbol{q})$, contains both the link and the motor inertia. In [15] it was shown that for the flexible joint robots like the DLR/KUKA LWR III the link inertia is decoupled from the motor inertia. In [1], the reflected robot mass was formulated as a function of the transmission stiffness

$$m_{\mathrm{r}}\left(K_J\right) = m_{\mathrm{link}} + \frac{K_J}{K_J+\gamma} m_{\mathrm{mot}}, \tag{4}$$

for the 1-DOF case[1], where m_{mot} denotes the motor inertia, m_{link} the link inertia, K_J the joint stiffness, and γ a design factor. Depending on K_J the reflected mass ranges from $m_r = m_{\mathrm{link}}$ (decoupled) to $m_r = m_{\mathrm{link}} + m_{\mathrm{mot}}$ (rigid). For planning safe motions in HRI applications the ISO/TS proposes a simplified model of the effective mass, namely

$$m_{\mathrm{r,ISO}} = M/2 + m_{\mathrm{L}}, \tag{5}$$

where M is the summed mass of all moving parts of the robot system and m_{L} is the payload [13]. Please note that (5) does not depend on the joint configuration in contrast to (2).

III. Effective mass distribution

In this section, we compare the effective masses obtained by (2) and the simplified model (5) for the reachable workspace of two exemplary robots, namely the FE Panda and the LWR IV+. No end-effector or payload is considered for both robots. We discretize the robots' reachable workspace by defining a position grid with $5\,\mathrm{cm}$ uniform distance, see Fig. 2 (top). We consider only one end-effector orientation, where the flange points downwards with the end-effector frame being axis-aligned with the world coordinate frame, see Fig. 2 (top left). For each position/pose in the workspace grid, we determine an associated joint configuration with the inverse kinematics algorithms [20] (LWR) and [17] (Panda). For every feasible pose/configuration we then evaluate the reflected mass in 20 uniformly distributed Cartesian directions $\boldsymbol{u}$. In Fig. 2 (top) we show the workspace grid for the LWR and Panda. The distribution of the reflected mass in the robots' workspace, i.e., the relative number of robot positions associated to a certain effective mass range is illustrated in the middle and bottom figure. Here, we also illustrate the reflected mass obtained by (5) (ISO/TS), which is simply found to be $m_{\mathrm{r,ISO}} = 5.545\,\mathrm{kg}$ for the Panda,

[1]Equation (4) may be extended to n-DOF via [16].

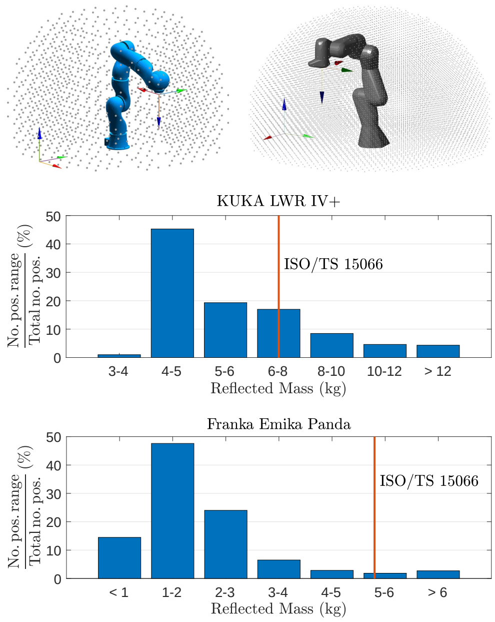

Fig. 2. Cartesian positions (top) and workspace reflected mass distribution for the KUKA LWR IV+ (middle) and Franka Emika Panda (bottom).

where we use the inertial parameters provided in [19], and $m_{\mathrm{LWR,ISO}} = 6.3\,\mathrm{kg}$ for the LWR. For the LWR it can be observed that in approx. $60\,\%$ of the reachable workspace the reflected mass is lower than the $6.3\,\mathrm{kg}$ obtained by ISO/TS. For the Panda, the reflected mass is lower than the simplified ISO/TS estimate in $97\,\%$ of the cases.

IV. Experimental Derivation of the Effective Robot Mass

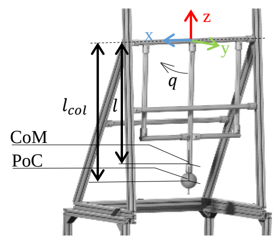

Fig. 3. Model of the pendulum's effective mass explained using it's CAD-model.

To investigate the robot effective mass experimentally, we consider the robot mass perceived during a collision with a pendulum based on the conservation of momentum

$$m_{\mathrm{p,eff}}\dot{y} = m_{\mathrm{r,exp}} v_{\mathrm{r}}, \tag{6}$$

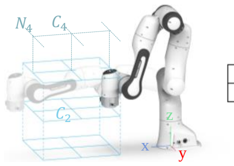

C_4	$[498, 0, 626]$ mm
N_4	$[698, 0, 626]$ mm

Fig. 4. ISO 9283 reference cube and extension for verifying the effective mass

where $\dot{y}$ is the pendulums instantaneous velocity after collision, $m_{\mathrm{r,exp}}$ the experimentally determined robots effective mass, v_{r} the robot velocity at the contact location.

A. Experimental setup

To obtain $m_{\mathrm{r,exp}}$ we use an experiment based on a passive physical pendulum which is shown in Fig. 3. We measure the instantaneous translational velocity $\dot{y}$ of the pendulum using a precision light barrier 203.10 and the measuring counter 373 by Hentschel. The robot velocity v_{r} at the contact location is obtained by the measured robot joint velocity, which is transformed to Cartesian space via $\boldsymbol{J}(\boldsymbol{q})$. The pendulum's effective mass at the point of contact is given by

$$m_{\mathrm{p,eff}} = \frac{J_{xx}^{(\mathrm{S})} + m_{\mathrm{p}} l^2}{l_{\mathrm{col}}^2}\,, \tag{7}$$

where $J_{\mathrm{xx}}^{(\mathrm{S})}$ is the inertia about the pendulum center of gravity, m_{p} the pendulum summed mass, $l = 636\,\mathrm{mm}$ the distance to the center of gravity, and $l_{\mathrm{col}} = 815\,\mathrm{mm}$ the distance to the point of collision. From CAD we obtain $m_{\mathrm{p,eff}} = 3.663\,\mathrm{kg}$.

We select the robot test poses based on the reference cube defined in DIN EN ISO 9283. To enable a collision with the horizontally oriented robot flange we extend the reference cube and also consider the Cartesian positions C_4 and N_4 illustrated in Fig. 4. The robot joint configurations associated to C_4 an4 N_4 are upon collision are

$$\boldsymbol{q}_{C4} = [-0.9, -9.5, 0.6, -129.8, 0.8, 210.1, 51.7]^{\mathsf{T}}\,^{\circ} \text{ and}$$
$$\boldsymbol{q}_{N4} = [-0.6, 11.9, 0.5, -92.6, 0.8, 184.8, 46.5]^{\mathsf{T}}\,^{\circ}.$$

We select a Cartesian robot motion along the x-axis starting close to the robot base and ending at the workspace boundary. When detecting a collision with the pendulum, the robot fully brakes triggered by the internal joint torque sensing. We use three different collision velocities: $200\,\mathrm{ms}$, $250\,\mathrm{ms}$, and $300\,\mathrm{ms}$.

In the experiment, the robot flange collides with the pendulum, we use the internal dynamics model of the Panda to calculate the effective mass according to [8] (cf. (2)) with the Cartesian direction being $\boldsymbol{u} = [1, 0, 0]^{\mathsf{T}}$.

B. Results

Our experimental results are depicted in Fig. 6. For C_4 we observe $m_{\mathrm{r,exp}} = 2.765 \pm 0.062$ kg, the difference w.r.t. (2) is $1.1\,\%$ ($m_{\mathrm{r}} = 2.797 \pm 0.003$ kg). In contrast, the error between $m_{\mathrm{r,exp}}$ and the ISO/TS effective mass $m_{\mathrm{r,ISO}} = 5.22\,\mathrm{kg}$ is

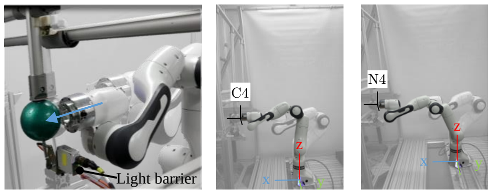

Fig. 5. Pendulum test set up to evaluate the effective mass of the robot using the depicted light barrier and a stopping mechanism at position C_4 (centre) and N_4 (right)

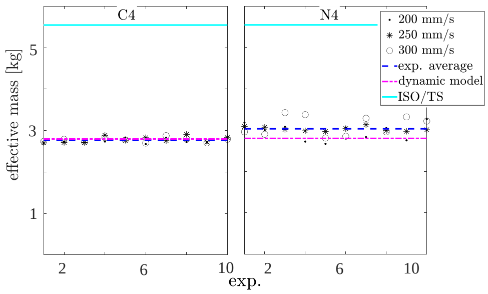

Fig. 6. Effective mass at the C_4 (left) and N_4 (right) position according to [13] (turquoise) and the experimentally derived effective mass (blue) with the corresponding values for the effective mass using [8].

$88.8\,\%$. We obtain similar results for the N_4 position, i.e. $m_{\mathrm{r,exp}} = 3.018 \pm 0.184$ kg in the experiment, $m_{\mathrm{r}} = 2.800 \pm 0.005$ kg via (2), and $m_{\mathrm{r,ISO}} = 5.222$ kg (ISO/TS) where the error between experiment and (2) is $7.8\,\%$ and $73.0\,\%$ between experiment and ISO/TS.

The error between experiment and (2) in our N_4 experiments is higher than in the C_4 experiment. This is presumably due to the preliminary experimental set up, which requires further calibration. Please also note that the Panda internal robot model is closed, i.e., not available to the authors, and may differ from the model used in Sec. III.

C. Usage of incorrect mass for safe velocity control: Implications on safety and performance

Inspired by [10], the ISO/TS provides safety curves which relate the instantaneous robot reflected mass to a maximum biomechanically safe velocity (pain threshold). Consider the following two undesired scenarios:

a) The actual robot mass is lower than the mass calculated according to ISO/TS. The commanded velocity is regarded as safe, but a higher safe velocity would be possible based on the actual robot reflected mass. In this case, productivity is deteriorated in terms of cycle time.
b) The robot reflected mass is larger than the one obtained by ISO/TS, the robot travels with a speed that is higher than the safety curve would allow based on the actual

mass. The safety thresholds may be violated, which potentially makes the application unsafe.

According to our results in Sec. III, case a) holds for $97\,\%$ of the workspace area of the FE Panda and for more than $60\,\%$ of the workspace of the KUKA LWR IV+. For these robots, the application of the ISO/TS reflected mass usually results in decreased productivity. However, also case b) is likely, meaning the safety thresholds can be exceeded. The authors therefore recommend to replace the effective mass model (5) in ISO/TS by the well-established formulation (2) [8] (as our experimental results agree well with the theory for the considered robots) or a data-driven relation between the robot configuration and the measured reflected mass.

V. Conclusion

The effective mass of a robot is known to have an important impact on the operator safety in case of a collision. In our experimental investigations we observed a significant difference between the simplified ISO model and the state of the art dynamic model that is well established in the robotics community since decades. The simplified model proves to be not only overly conservative in most cases, thereby limiting the robot's efficiency and economic use, but it may also lead to an underestimation of hazard, which can jeopardize human safety in HRI applications. Therefore, we suggest for every collaborative robot to provide and use an accurate dynamics model for appropriate real-time safety control and reliable safety assessment.

Acknowledgment

The authors would like to thank Johanna Wolff for her preparatory work. This work was supported by the European Union's Horizon 2020 research and innovation programme as part of the project ILIAD under grant no. 732737 and partially supported by the Research Project I.AM. through the European Union H2020 program under GA 871899. We gratefully acknowledge the funding of the Lighthouse Initiative Geriatronics by StMWi Bayern (Project X, grant no. 5140951) and LongLeif GaPa gGmbH (Project Y, grant no. 5140953). Please note that S. Haddadin has a potential conflict of interest as shareholder of Franka Emika GmbH.

References

[1] A. Bicchi and G. Tonietti, "Fast and "soft-arm" tactics," in IEEE Robotics & Automation Magazine, vol. 11, no. 2, pp. 22-33, June 2004.

[2] R. Behrens and N. Elkmann, "Study on meaningful and verified Thresholds for minimizing the consequences of human-robot collisions," 2014 IEEE International Conference on Robotics and Automation (ICRA), Hong Kong, 2014, pp. 3378-3383.

[3] S. Haddadin, A. Albu-Schffer, O. Eiberger and G. Hirzinger, "New insights concerning intrinsic joint elasticity for safety," 2010 IEEE/RSJ International Conference on Intelligent Robots and Systems, Taipei, 2010, pp. 2181-2187.

[4] K. Suita, Y. Yamada, N. Tsuchida, K. Imai, H. Ikeda and N. Sugimoto, "A failure-to-safety "Kyozon" system with simple contact detection and stop capabilities for safe human-autonomous robot coexistence," Proceedings of 1995 IEEE International Conference on Robotics and Automation, Nagoya, Japan, 1995, pp. 3089-3096 vol.3.

[5] S. Haddadin, A. Albu-Schäffer, G. Hirzinger, "Safety Evaluation of Physical Human-Robot Interaction via Crash-Testing." Robotics: Science and systems, vol. 3, 2007.

[6] K. Ikuta, H. Ishii, M. Nokata, Safety Evaluation Method of Design and Control for Human-Care Robots. The International Journal of Robotics Research. 2003;22(5):281-297.

[7] O. Khatib, "A unified approach for motion and force control of robot manipulators: The operational space formulation," in *IEEE Journal on Robotics and Automation*, vol. 3, no. 1, pp. 43-53, February 1987.

[8] O. Khatib, "Inertial Properties in Robotic Manipulation: An Object-Level Framework." *The International Journal of Robotics Research*. 1995;14(1):19-36.

[9] D. Walker, "The use of kinematic redundancy in reducing impact and contact effects in manipulation", Robotics and Automation 1990. Proceedings. 1990 IEEE International Conference on, pp. 434-439, 1990.

[10] S. Haddadin, S. Haddadin, A. Khoury, T. Rokahr, S. Parusel, R. Burgkart, A. Albu-Schäffer, "On making robots understand safety: Embedding injury knowledge into control", *The International Journal of Robotics Research*, vol. 31, 13th ed, 2012, pp. 1578-1602.

[11] D. Kulić, E. Croft, "Pre-collision safety strategies for human-robot interaction." Auton Robot, vol. 22, 2007, pp. 149164.

[12] N. Mansfeld, B. Djellab, J. R. Veuthey, F. Beck, C. Ott and S. Haddadin, "Improving the performance of biomechanically safe velocity control for redundant robots through reflected mass minimization," 2017 IEEE/RSJ International Conference on Intelligent Robots and Systems (IROS), Vancouver, BC, 2017, pp. 5390-5397.

[13] ISO/TS 15066:2017, *Robots and robotic devices - Collaborative robots*, Beuth-Verlag, Berlin.

[14] T. Lens and O. von Stryk, "Investigation of safety in human-robot-interaction for a series elastic, tendon-driven robot arm," 2012 IEEE/RSJ International Conference on Intelligent Robots and Systems, Vilamoura, 2012, pp. 4309-4314.

[15] S. Haddadin, et al. Requirements for Safe Robots: Measurements, Analysis and New Insights. The International Journal of Robotics Research, vol. 28, no. 1112, Nov. 2009, pp. 15071527.

[16] A. Albu-Schaffer, M. Fischer, G. Schreiber, F. Schoeppe and G. Hirzinger, "Soft robotics: what Cartesian stiffness can obtain with passively compliant, uncoupled joints?," 2004 IEEE/RSJ International Conference on Intelligent Robots and Systems (IROS) (IEEE Cat. No.04CH37566), Sendai, 2004, pp. 3295-3301, vol.4.

[17] P. Corke, Robotics, vision and control: fundamental algorithms in MATLAB second, completely revised. Vol. 118. Springer, 2017.

[18] W. J. Stronge, "Impact mechanics." Cambridge university press, 2018.

[19] C. Gaz, M. Cognetti, A. Oliva, P. Robuffo Giordano and A. De Luca, "Dynamic Identification of the Franka Emika Panda Robot With Retrieval of Feasible Parameters Using Penalty-Based Optimization," in IEEE Robotics and Automation Letters, vol. 4, no. 4, pp. 4147-4154, Oct. 2019.

[20] R. Konietschke, Planning of Workplaces with Multiple Kinematically Redundant Robots, Technical University of Munich, 2008.